QATAR UNIVERSITY

COLLEGE OF ENGINEERING

DEVELOPMENT OF NOVEL INSTRUMENTATION INCORPRATING MAGNETORESISTIVE ENCODERS FOR THE MEASUREMENT OF ANGULAR POSITION AND SPEED

BY

SHARIEF SALEH

A Thesis Submitted to

the Faculty of the College of

Engineering

in Partial Fulfillment

of the Requirements

for the Degree of

Masters of Science in Electrical Engineering

June 2018

COMMITTEE PAGE

The members of the Committee approve the Thesis of Sharief Saleh

defended on 14/05/2018.

_____

Mohieddine Benammar
Thesis/Dissertation Supervisor

_____

Farid Touati
Committee Member

_____

Faical Mnif
Committee Member

Approved:

_____

Khalifa Al-Khalifa, Dean, College of Engineering

ABSTRACT

SALEH, SHARIEF, E., Masters :

June : 2018, Masters of Science in Electrical Engineering

Title: Development of Novel Instrumentation Incorporating Magnetoresistive Encoders for The Measurement of Angular Position and Speed

Supervisor of Thesis: Mohieddine, A, Benammar.

As rotation dependent technologies emerge, the need of having a feedback about their rotational behavior became a necessity in order to control them. Many types of sensors, based on various operation principles are available in the market to provide such feedback. One of these sensors are sinusoidal magneto resistive (MR) type sensors. Such sensors have many merits over other angular position sensors, yet extracting the angle of interest, θ, from their signals is not a trivial task as they encode the angle into two orthogonal sinusoidal signals. Furthermore, these signals also suffer from imbalances and imperfections in practice. Towards extracting the angle from the sensor signals and minimizing the effects of their imperfections, a thorough literature survey has been conducted to learn about the state of the art linearization techniques. Despite that the extraction of angle from the orthogonal sensor signals can be based on open loop or closed loop techniques, all of the work on MR sensors is based on open loop techniques. The latter methods are not as robust as closed loop techniques. Towards filling such gap, a novel closed loop technique based on the well-known Phase Locked Loop (PLL) technique is proposed. The enhanced PLL eliminates the need of analog multipliers; needed in the Phase Detector stage, through the exploitation of the resistive nature of the MR sensors. Subsequently, novel imbalance correction techniques are proposed to suit the proposed

enhanced PLL converter. The theory of the proposed techniques is discussed in detail along with extensive simulations and practical implementation to test their performance. It is shown practically that the proposed enhanced PLL and imbalance correction techniques perform as expected, as the enhanced PLL technique showed identical performance to that of a classical PLL, and the proposed imbalance correction techniques successfully eliminated the present imbalances. Experimental results show that both proposed and classical PLL methods resulted in around 1.2° Peak-Peak error over the whole 360° range. The error was then shown to be caused by a 3rd harmonic distortion from the sensor's side and not the proposed method.

DEDICATION

Dedicated to

My beloved family,

The person who is soon to be my wife

&

The Godfather of Instrumentation, Prof. Mohieddine Benammar

ACKNOWLEDGMENTS

First and foremost, I thank **Allah (GOD) Almighty** for bestowing his many blessings upon me and granting me the will, strength, and patience to fulfill this work.

My dear **parents** and my 11 years old genius brother, **Omar**. I was blessed to have your continuous, selfless and unfailing support for the past years! No words may ever express my gratitude towards you. Father and Mother, I believe that this work is one fruit of many more yet to come as a result of your great parenting for the past 23 years. Omar, thanks for entertaining me throughout the whole period while working on my thesis. Gaming and chatting with you brought me a lot of happiness and kept me entertained enough to finish this work! Thank you, brother!

Mariam, my beloved fiancé, future wife and my emotional supporter. I can not thank you enough for the many times you kept listening while explaining to you my thesis and the technical hardships I was facing. It was hilarious how you kept up with these conversations although it is not your field of study. Thanks for all the food you brought me while I was oversleeping at university to finish my thesis. It was delicious!

Prof. Mohieddine Benammar, my dear and beloved mentor. Your door was always open to me at any time, day and night, working days as well as holidays. Your wisdom is beyond description. You granted me the privilege of climbing the learning curve on my own while keeping a close eye to steer me to the right direction whenever you felt needed. I had the honor of working by your side and learn from your great reservoir of experience in research, teaching and even life, you are my role model and hero, professor!

TABLE OF CONTENTS

LIST OF TABLES

LIST OF FIGURES

CHAPTER 1: INTRODUCTION

Many modern technologies such as robotics, satellites and machines, adopt rotational motion as an essential mechanism within their respective systems. Controlling such technologies accurately with adequate dynamic response usually lead to many of benefits within their respective fields. For example, accurate and relatively fast response control of assembly line robotics would lead to efficient assembly lines and would improve yield and benefits. Also, precise control of solar panels to direct them towards the sun would in return harvest more energy. On the other hand, failing to control some of these rotational motion-dependent technologies either accurately or in rapidly would sometimes lead to catastrophes. A good example of that would be robotic surgeries, where a minute error or a delayed response would lead to fatal consequences on the patient's behalf. Many other applications depict such sensitive dependency on rotational motion control, such as avionics, military applications, autonomous vehicles, and electric machines.

In order to have a precise control over a rotating object, two main objectives shall be fulfilled, a well-designed control algorithm and an accurate / fast response feedback. The feedback is usually done with information obtained from angular position / displacement sensors attached to the actuators. These sensors convert the angular position θ and possibly the speed $\frac{d\theta}{dt}$ into equivalent electrical signal(s) either in linear or a non-linear relationship. Many angular position sensors are available in the market with many different operation principles, advantages and disadvantages. These sensors can be classified into: Capacitive [1]–[3], Inductive [4]–[6], Hall-Effect [7]–[9], Optical Encoders [10], [11][12] and Magneto Resistive [13]–[15].

1.1 Angular Position Sensors

As the name suggests, capacitive angular position sensors depend on the capacitors with specific arrangements to detect the angle. Capacitance of capacitors are governed by the well-known equation

$$C = \frac{\varepsilon A}{d} \tag{1.1}$$

Where ε is the permittivity of the dielectric material between the plates, A is the total area of overlap between the two plates and d is the distance between the two plates. Capacitive sensors usually have one or more of the aforementioned variables changed with respect to the change of the angular position of the rotating object. For example, the two plates can be manufactured to have one half of the plate to be made out of conducting material, and the second half to be a non-conducting material, and thus, by fixing one plate and connecting the second to the rotating object, the overall area of overlap between the two plates will change depending on the position of the rotating plate. Now, in order to have a measurement of the angle, one should first find the relationship between the varying angle θ and the varying capacitance C. If the capacitor plates were set to be having alternating conductive halves at $\theta = 0°$, Then, the initial area of overlapping is Zero. The area of overlapping will then increase as the rotating object rotates away from the initial position, until both conducting materials are overlapping fully. The increase of the area of overlapping is proportional to the angle of deviation from the initial point. The area of overlapping may then considered to be the area of a sector, which is a ratio of the angle θ to the whole 2π range multiplied by total area of the circle as shown in (1.2):

$$A_{overlapping} = \frac{\theta}{2\pi} \times (\pi \cdot r^2) = \frac{\theta}{2} \cdot r^2 \quad (1.2)$$

Which is a linear relationship with respect to the angle of interest, θ. Thus, by combining Equations (1.1) and (1.2) the capacitance will now be:

$$C = \frac{\varepsilon(\theta r^2)}{2d} \quad (1.3)$$

Where r is the radius of the plates. It is worth mentioning that such scheme will suffer from ambiguity of differentiating between angles before and after $\theta = 180°$. After knowing the relationship between the capacitance and the angle of the rotating object, a circuitry should be designed to translate that capacitance change into a signal to infer the angle of interest, θ. A good example of that is Wien bridge. Capacitive sensors have many advantages. As they possess a linear relationship with the angle of interest θ. They operate in a contactless manner and they can operate at very low power levels. Their main problem resides in being very hard to manufacture and noise attractive as they are highly affected by parasitic capacitances.

Inductive angular sensors, such as resolvers, however, consist mainly of two parts, a rotor and a stator. Resolvers act as a rotating transformer. The rotor is to be connected to the rotating object and is usually excited by an AC signal $A\sin(\omega t)$ through its windings, where A and ω are the amplitude and the angular frequency of excitation signal respectively. On the other hand, the stator got two windings wound around it that are $90°$ mechanically apart. Thus, the excited rotor will induce an AC sinusoidal current through the stator's windings modulated by the sine and the cosine of its instantaneous angular position multiplied by the transformation factor between the windings T. Thus, the output

of the resolver can be expressed as:

$$V_s = A\,.T\,sin(\omega t)\,sin(\theta) \tag{1.4}$$

$$V_c = A\,.T\,sin(\omega t)\,cos(\theta) \tag{1.5}$$

The main advantage of resolvers is that they are rugged and very robust against harsh environments, and have immunity towards vibrating environments as well as dusty ones, which makes it very ideal in industrial applications. Yet, they have the main drawback of producing outputs that have a non-linear relationship with the angle of interest θ, thus, they need adequate converters to linearize them. Also, they have a modulated output, thus, in most cases, they need demodulators in order to be able to detect the enveloping sinusoidal function of θ, as well as their relatively high price.

Optical encoders have a very different operating principle, as they consist of three parts, photo transmitter, photo receiver and a mechanically moving device made out of two materials, a light blocking material and a light passing material. This device is found between the transmitter and the receiver and rotates with the rotating object. The device is divided into N equally spaced sectors. The body of each sector will consist of the light blocking material while the borders between each sector will consist of light passing material. Thus, the photo transmitter's light will be blocked from passing to the receiver most of the time but at the borders between the sectors. Therefore, optical encoders divide the whole $360°$ angular space into N discrete levels. Within those levels, the output; from the photo receiver's side, would be Null most of the time. Yet, at the border between each level and the other, the sensor produces an impulse. As a result, in order to know the current angle of the rotating objects, one should count the number of pulses produced by the sensor

from a reference position to the current moment, then multiply that number by $\frac{360^\circ}{N}$ to get the final angle. What makes Optical Encoders superior is their high accuracy, their outputs can be processed easily to get the angle of interest θ, and they measure it in a contactless manner. Yet, unlike Resolvers, they are usually disregarded when the application is expected to be operating at harsh environments, as they are highly vulnerable and weak towards mechanical shocks, vibrations and high temperatures.

As the name suggests, Hall effect sensors utilize the Hall principle introduced by Mr. Edwin Herbert Hall in 1879, to detect the angular position of rotating objects. The Hall effect happens when a magnetic field come into proximity to a current carrying material, as it then forces the electrons to be pushed towards one end of the conducting material, producing a small voltage difference within that conducting material. Now, the amount of voltage produced is proportional to the intensity of the magnetic field felt by the material. Thus, Hall effect angular position sensors exploit this dependency by attaching a magnet to the rotating object, and as it rotates, the magnet will be at different distances away or close to the material depending on the angular position. Therefore, the magnetic field intensity will vary with the rotation, and so does the voltage emerging across the conducting material. It can be seen that the relationship between the angular position and the voltage developed will be proportional to $\sin(\theta)$. Thus, by attaching another conducting material that is 90° mechanically apart from the first material, the sensor will be able to output a two quadrature signals, namely $\sin(\theta)$ and $\cos(\theta)$. Usually, the voltage developed across these materials will be very small, in the range of microvolts, and thus, most of them have internal high gain amplifiers to boost them to considerable voltage

levels. Hall Effect sensors are very popular for their high accuracy, low power operation, contactless measurement scheme. Yet, their main disadvantage is their output's nonlinear relationship to the angle of interest θ as well as its dependency on the magnitude of the magnetic field, which makes is vulnerable to magnetic interference.

Last but not least, magneto resistive (MR) encoders are another class of angular position sensors. Magneto resistance materials are materials that has their electric resistance affected by the magnetic field's position relative to them. Thus, by attaching a strip of magnetic material to the rotating object; i.e. Permanent Magnet (PM), and then have the MR sensor faced towards it, the resistance of that MR material will vary in a sinusoidal manner with respect to the angular position. The resistance of the MR material can be governed by the following equation (1.6):

$$R = R_{min} + \frac{\Delta R}{R_{min}} * X(\theta) \tag{1.6}$$

Where $\frac{\Delta R}{R}$ is the sensitivity ratio of the MR sensor, and $X(\theta)$ is a sinusoidal function of θ; either $\cos(\theta)$ or $\cos^2(\theta)$ depending on the MR type, which will be discussed in detail in the next chapter. Thus, the resistance will vary with the angular position θ in a sinusoidal fashion. Similarly, to the Hall-Effect sensors, MR materials can be arranged to be mechanically separated by 90° to produce quadrature signals at the output. There are many magneto resistive technologies proposed, some of which will be discussed in the next chapter. MR sensors exhibit much of the advantages and disadvantages of the Hall Effect sensors, as they operate at low power levels, they measure the angle in a contactless manner, they can be very accurate depending on the MR technology employed. Likely, they possess the same non-linear relationship towards the angle of interest θ. Yet, their

advantage over Hall effect sensors relies on the fact that they depend on the angle of the magnetic field rather than its intensity, and thus, the are less vulnerable towards magnetic interference. Also, perhaps, their greatest advantage over all other angular position sensors is their very small size and weight. As they may span only couple of millimeters in dimension as opposed to others, which makes them a perfect fit for small sized applications were other sensors can't usually fit.

Going through some of the most famous angular position sensors, it can be observed that they can be classified into two categories, sinusoidal and non-sinusoidal sensors. For example, inductive, Hall-Effect and MR sensors exhibit a sinusoidal relation between the angle of interest θ and the output signals. While on the other hand, capacitive and optical encoder sensors do exhibit linear relationship instead. Of course, linear sensors have a clear advantage over non-linear / sinusoidal sensors in terms of complexity of extracting the angle out of the output signal as well as the uniform sensitivity over the $360°$ range of operation. Yet, sinusoidal sensors may sometimes have better characteristics at other aspects of instrumentation such as robustness towards vibration noise, operativity under harsh environment, contactless measurements, low power operation, small physical size and weight and many others. Table 1.1 summarizes a comparison among various types of angular position sensors compiled from the pros and cons of each sensor. The shaded areas are the advantages of each sensor. From the table, MR sensors have a clear advantage over the other sensors in many criteria, and thus is the chosen sensor.

Table 1.1 Comparison between angular position sensors

Level	Easiness to Decode	Robustness (Elec/Mech)	Physical Size and Weight	Power Consumption	Price / Complexity
Capacitive	Linear	Vulnerable to noise	Mid-range	Low	Complex
Inductive	Sinusoidal and modulated	Robust and rugged against harsh environment	Large and heavy	High	High price
Hall-Effect	Sinusoidal	Vulnerable to magnetic interference	Mid-range	Very low	High price
Optical Encoders	Counter based	Weak towards mechanical shocks	Small	Mid-range	Mid-range
Magneto Resistive	Sinusoidal	Robust against magnetic interference as well as mechanical shocks	Very Small	Very low	Mid-range

1.2 Problem Description

Given that the sensor type of choice was MR sensors, then two main issues will need to be dealt with. First, an adequate converter will be needed to detect and extract the angular position θ out of the encoded sinusoidal signals. At a first glance, one might think of using the well-known CORDIC method to calculate the angle by taking the inverse

trigonometric function of these sinusoidal signals; i.e. $\sin^{-1}(\sin(\theta)) = \theta$. Yet, this primal method would run into problems for many reasons. First, it is very hard to construct an analog circuitry to compute the inverse sine function. Second, if such computation is to be done digitally, Look Up Tables (LUTs) will be used to undertake this task, and thus, the resolution of the converter will heavily depend on the size of the LUT used, which will lead to very high errors if a small sized LUT was available. Third, not having a feedback would leave the system vulnerable to stability issues. That's why many alternative conversion solutions were proposed. Such conversions come at the cost of having an error and time delay within the control loop, thus, many algorithms and circuitries were proposed in the literature to optimize conversion techniques to come up with the least error while maintain fast dynamic response and relatively low complex solution. Towards that, a novel closed loop converter will be proposed in the later chapters that will lower the complexity of an already will-known closed loop converter.

Second, sinusoidal signals might be imbalanced in different ways and due to different reasons, such as sensors ageing effect, or initial misalignment, etc. [16]–[18]. Imbalances might come in the form of amplitude imbalance, DC shift imbalance and/or phase imbalance between the quadrature signals of the sensor. Thus, the output signals of the sensors can be written as:

$$V_{Sin} = A(1+\alpha)\, sin(\theta + \phi) + DC_{Sin} \tag{1.7}$$

$$V_{Cos} = A \cdot cos(\theta) + DC_{Cos} \tag{1.8}$$

Where A is the balanced amplitude of the sine and cosine, α is the amplitude imbalance, ϕ is the phase shift imbalance and DC_{Sin} and DC_{Cos} are the DC shift imbalances

of sine and cosine respectively. These imbalances may happen individually, and thus, they can be detected and corrected easily, or simultaneously, therefore, the detection algorithm would be much more complicated. If these imbalances were not detected and compensated for, they will affect the instrumentation drastically, and many errors will evolve. Thus, adequate imbalance correction techniques will be proposed to adapt with the proposed converter.

1.3 Scope

The scope of this thesis focuses on the two main concerns related to sinusoidal encoders instrumentation systems. First, MR sinusoidal to angular position converters. Second, correction techniques. The thesis will report relevant state-of-the-art techniques reported in the literature regarding MR converters. Then, it would proceed to contribute in both domains by 1) proposing an enhanced closed loop converter that lowers the complexity of a well-known closed loop converter in a novel way. 2) proposing adequate imbalance correction technique to suit the proposed converter. Other limitations within the angular position instrumentation systems are as important as the two aforementioned issues, yet they are considered to be out of the scope of this work.

1.4 Objectives

The objectives of this thesis are to 1) study and review thoroughly the relevant works regarding MR sinusoidal to angle converters, 2) Propose a novel sinusoidal to angle converter for MR sensors, 3) Propose a novel correction technique that suits the proposed

converter, 4) Practically implement and test the proposed methods.

1.5 Outline

This thesis started with an introduction that briefly highlighted the need of angular position measuring instruments as well as the criteria upon which they should be built. Followed by a brief introduction to the most known sensors categories that undertake such measurements along with a comparison between them while highlighting the importance of sinusoidal encoders and MR sensors in particular. Then, it discussed their main problems and areas of research as well as the scope, objectives and the outline of the thesis (Chapter 1). In Chapter 2, magneto resistive angular position sensors will be discussed in detail followed by a literature survey that views the state of the art advances in conversion techniques employed to linearize their outputs. Chapters 3 and 4 discuss the theory of the proposed novel MR converter and imbalance correction techniques along with their simulations and practical implementation respectively. Finally, Chapter 5 draws the conclusions of this work, states the limitations of the proposed methods and adds a comment on the future work that could be used for further improvements.

CHAPTER 2: MAGNETO RESISTIVE SENSORS

2.1 History

In 1856, Lord kelvin discovered a strange behavior when he subjected a current carrying iron bar to a magnet, as he discovered a change in the iron bar's resistance. The resistance of the iron bar increased to its maximum when the magnetic field was in parallel to it, and reduced to its minimum when the magnet was perpendicular to it. Because of such orientation dependent phenomena, the effect was given the name anisotropic magnetoresistance (AMR)[19]. He did then test with other materials like Nickle and found the same behavior, but with a more prominent effect. A hundred years later, Fert and Grünberg were experimenting with multilayers of iron and chromium (Fe/Cr). Fert was conducting his experiments at $4.5K$ temperature while Grünberg was experimenting at room temperature. Both found out that by changing the thickness of the nonferromagnetic material, Chromium in this case, as well as changing the temperature of operation had a significant effect on the change in the resistance, which peaked at 50%. Accordingly, Fert gave it the name Giant Magnetoresistance (GMR)[20], [21]. In 2007, they received a Nobel prize for their work. Few years earlier, Jullière was experimenting with Fe/Ge-O/Co junctions at $4.2K$ and found a maximum change of 14% in the resistance when the junctions were subjected to a magnetic field. He interpreted such behavior as electrons tunneling through the thin junctions to the other side, hence the name Tunneling Magnetoresistance (TMR)[22]. Years later, researchers were able to achieve higher amounts of change in resistance by experimenting with different materials as they exceeded 1000% change of resistance [23], [24]. As of today, TMR is considered to be the best of

the three technologies in term of sensitivity towards surrounding magnetic field.

2.2 Principle of Operation

AMR effect is a result of a directed magnetic field interacting with the spin of the electrons within a ferromagnetic material, which increases or decreases their s-d scattering depending on the direction of the magnetic field with respect to the material [25]–[27]. An increase in the scattering would increase the resistance of the material and vice versa. Each material has its own MR effect ratio, yet all of them behave the same against a rotating magnetic field. As all of them would have a specific amount of minimum resistance; R_{Min}, without having a magnetic field in their vicinity. If the magnetic field was perpendicular to the current passing through the ferromagnetic material, then it will have no effect on it, as no scattering will occur, and thus, the resistance will remain at its minimum; $R_{Min} = R_{Perpendicular}$. On the other hand, by tilting the magnetic field away from the perpendicular position, its effect on the material will be more prominent, as more scattering will emerge, and thus, the resistance of the material will increase, until it reaches its maximum when the magnetic field is in parallel to it; $R_{Max} = R_{Parallel}$, [25]–[30]. The Resistance of the AMR sensor is expressed as:

$$R = R_{Min} + \frac{R_{Max} - R_{Min}}{R_{Min}} \times \cos^2(\theta) \tag{2.1}$$

The difference between the maximum and the minimum resistance relative to the minimum resistance is expressed as the MR ratio. The higher the MR ratio, the higher the sensitivity of the MR sensor towards the angular rotation of the magnetic field. In AMR sensors, MR ratio is around $3 - 5\%$ [25], [26], [29], [30].

GMR sensors on the other hand depend on having multilayers of ferromagnetic and non-ferromagnetic materials. The base and top materials are ferromagnetic while the non-ferromagnetic material is sandwiched in between. The base layer is called the pin layer, as it has a fixed magnetization direction, while the top layer is often called the free layer, as its magnetization direction depend on the surrounding magnetic field direction [26], [27], [29]–[31]. Without having a magnetic field in the vicinity of the GMR, the free and pin layers' magnetic fields are $180°$ out of phase, thus, the scattering would be at its maximum, which leads to the highest resistance, $R_{Max} = R_{Antiparallel}$. Tilting the magnetic field would then decrease the scattering, which will lead to a decrease in the resistance until it reaches its minimum at parallel position; $R_{Min} = R_{Parallel}$, [26], [27], [29]–[31]. By having multilayers, GMR sensors' maximum-minimum resistance distance increased, and thus, their sensitivity increased [26], [27], [29]–[31]. Likewise, TMR sensors consist of the same topology while replacing the non-ferromagnetic material with a thin insulator barrier/junction of around $(5 - 8)$ atoms in thickness [30], [32], [33]. This way, if no magnetic field was applied to the sensor, it will be very hard for the electrons to tunnel through the junction to create current, as the pin layer and the free layers are $180°$ out of phase, which will lead to even higher maximum resistance, which is in fact the main reason behind the high sensitivity of TMR sensors compared to the other sensors [30], [33].

The resistance of the TMR sensor as a function of the angular position of the rotating magnetic field can be expressed as:

$$R = R_{min} + \frac{\Delta R}{R_{min}} \times \cos(\theta) \tag{2.2}$$

2.3 Magnetoresistance interfacing

Usually, in order to have an idea about the direction of rotation, a quadrature output is needed. That's why, in most MR sensors technology kits, MR sensors are placed 90° physically apart from each other, so that, the change in their electrical resistance would be 90° shifted apart. Half bridges can be utilized with the aid additional two sensors to have a voltage division between the MRs, which will output two quadrature signals that are proportional to the angular position, θ. With regards to power of operation, MR sensors are just resistive, thus, they do not require a minimum power to operate. Therefore, their bridges can be powered through either AC or DC signals.

The MR sensors used in the related works and in the practical setup is produced by NVE, it incorporates four TMR sensors of $1.25M\Omega$ that are 90° physically shifted apart and are connected through double half bridges scheme, where each bridge is powered independently. The maximum supply voltage is $V_{cc} = 5.5V$, the sinusoidal output has a peak-to-peak voltage $V_{PP} = \pm 200\, mV/V$ and an offset of $V_{Offset} = \pm 10\, mV/V$ [34]. The outputs of the sensor are then:

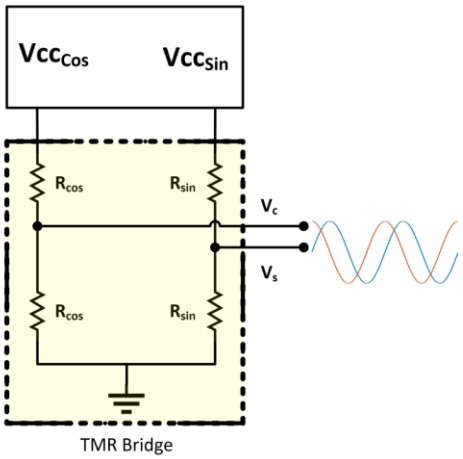

Figure 2.1. TMR sensor model

$$V_{Sin} = V_{CC_{sin}}\left(\frac{V_{PP_{Sin}}}{2} \cdot sin(\theta) + 0.5 + V_{Offset}\right) \tag{2.3}$$

$$V_{Cos} = V_{CC_{cos}}\left(\frac{V_{PP_{Cos}}}{2} \cdot cos(\theta) + 0.5 + V_{Offset}\right) \tag{2.4}$$

2.4 Literature Review

A literature survey was undergone to investigate the state of the art angle to digital converters used for MR sensors. It was found that very few papers were published in that field, and all of them were authored by the same research group. They published around nine publications proposing different converters for AMR, GMR and TMR sensors. Most of them are based on one main idea of angle conversion technique, yet, each paper solves some of its drawbacks and build on the previous ones. Each of these papers will be discussed in detail.

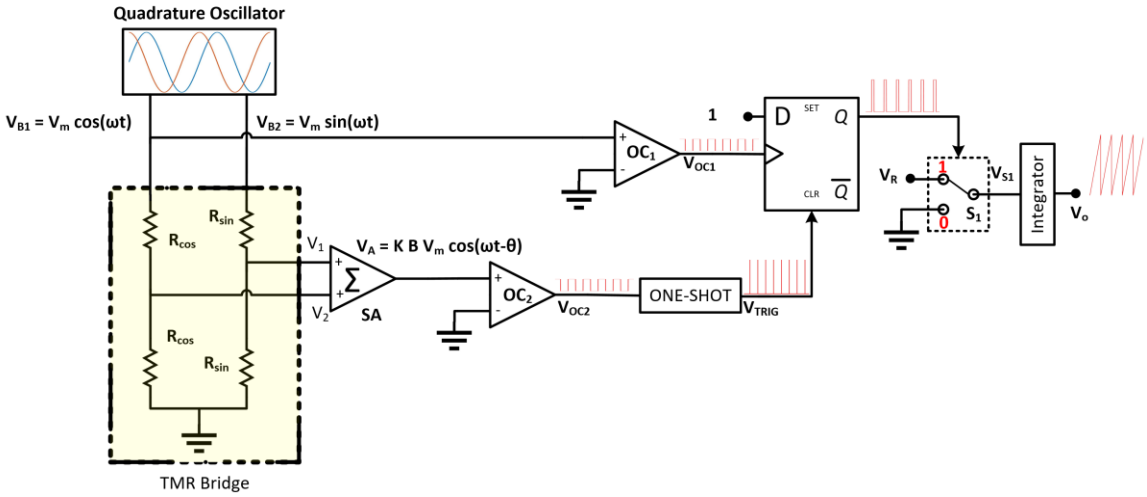

Figure 2.2. The proposed convertor in [35], [36]

The first publication was [35]. 3 years later, they published [36], which explains [35] in more detail. They proposed to have the TMR sensor powered through two quadrature signals, namely:

$$V_{B1} = Vm\, cos(\omega t) \tag{2.5}$$

$$V_{B2} = Vm\ sin(\omega t) \tag{2.6}$$

Generated by a quadrature oscillator. Thus, the outputs of the TMR sensor will be:

$$V_1 = KB\, V_m\, cos(\omega t)\, cos(\theta) \tag{2.7}$$

$$V_2 = KB\, V_m\, sin(\omega t)\, sin(\theta) \tag{2.8}$$

Where K is the transformation constant of the TMR half-bridge and B is the flux density of the Permanent Magnet (PM). Then, V_1 and V_2 are summed through a summing amplifier to produce:

$$V_A = KB\, V_m\, cos(\omega t - \theta) \tag{2.9}$$

Which is a phase shifted version of V_{B1}. Next, V_{B1} and V_A will be the input of two comparators to produce two square waves of fundamental angular frequency $= \omega t$ and are phase shifted by θ apart from each other, namely V_{OC1} and V_{OC2} respectively. These two signals will be utilized later. After that, they have a positively edge triggered D-Type Flip-Flop, that has its D terminal connected to HIGH. V_{OC1} is then utilized as a clock signal to the flip-flop. Thus, the output of the flip-flop will always return to HIGH whenever V_{OC1} gets triggered. On the other hand, V_{OC2} is inputted to a ONE-SHOT circuit, a monostable oscillator, that would produce a pulse whenever V_{OC2} triggers, at $\omega t - \theta = 270°$, to produce a trigger impulse V_{Trig}. That impulse, V_{Trig}, is then connected to the RESET terminal of the flip flop to turn the output Q to LOW. Thus, the output of the flip flop will turn HIGH when the clock is triggered and will remain HIGH during the phase shift period between the two signals V_{OC1} and V_{OC2}, until the V_{OC2} triggers V_{Trig}, which in turn invokes the RESET terminal and thus, the output Q resets to LOW again. Therefore, the period at which the output of the flip flop, Q, remains HIGH will directly depend on the phase shift θ, the angle of interest. The output of the flip flop, Q, is then utilized to control a Single-Pole Double-Throw (SPDT) switch which switches between either Ground or V_r, a reference voltage. The output of the switch, V_{S1} is then integrated to produce the final output:

$$V_o = \frac{1}{T}\int_0^T V_{S1}\, dt \; = V_R \left(\frac{t_1}{T}\right) = \frac{V_R}{360°}\, \theta \tag{2.10}$$

Where $T = \frac{2\pi}{w}$ and $t_1 = \frac{\theta}{w}$, the time delay between V_{OC1} and V_{OC2}. Therefore, the output will be a linear function of θ and depends only on V_R, the reference voltage. Thus, it does

not depend on the either K or B. Which means that if the MR sensor gets faulty, a new MR sensor can replace it without the need to re-calibrate the sensor as the transformation constant K would generally be slightly different among different MR sensors. Also, it means that the converter is immune to vibrations which would lead to slight variations in the magnetic flux B. The maximum error obtained for this method through simulations was 0.004%, and it decays linearly as the angle increases from 0 to 360°. The error was caused from the delays introduced by the one-shot and the flip-flop. The maximum error of the conditioning circuit alone practically was 0.15% and the overall error of the whole system was $\pm 1\%$.

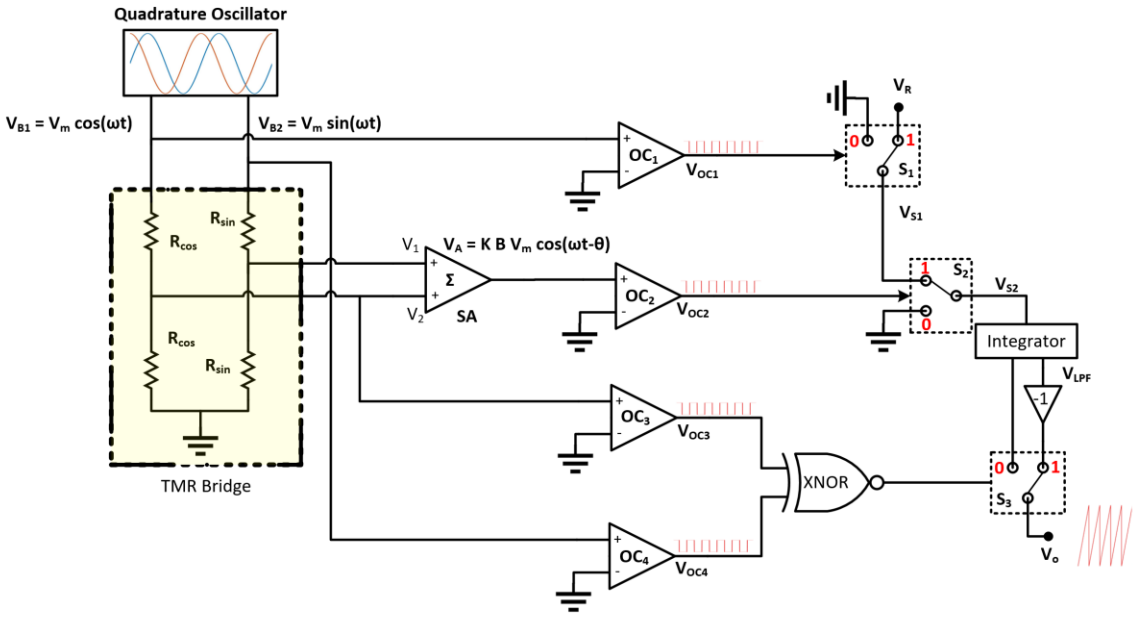

Figure 2.3. The proposed convertor in [37]

In [37], the authors built upon the idea proposed is [35] to further decrease the overall instrumentation measurement error. As in [35], the TMR sensor was powered through a quadrature oscillator. Then, the modulated sensor's output is summed through a summing amplifier to produce:

$$V_A = KB\, V_m\, cos(\omega t - \theta) \tag{2.11}$$

V_A along with V_{B1}, V_{B2} and V_2 pass through a phase detector circuit, which consists of 4 comparators and 3 SPDT switches and an integrator, to detect the angle of interest, θ, and output a voltage that is linearly related to it. The proposed phase detector circuit works as follows. V_A and V_{B1} are compared to the ground to output two square waves that are phase shifted by θ, V_{OC1} and V_{OC2}. V_{OC1} controls the first SPDT switch which switches between Ground or V_R, which then produces a signal V_{s1}. V_{OC2} controls the second SPDT switch which switches between Ground and V_{s1} and outputs a signal V_{s2}. Thus, $V_{s2} = V_R$ when V_{OC1} AND V_{OC2} are both HIGH. Else, $V_{s2} = 0$. It is worth reminding that V_{OC1} and V_{OC2} have the same square wave form yet with a phase shift of θ, thus, when V_{OC1} is HIGH, V_{OC2} will be also HIGH except for the period of the phase shift. This means that V_{s2} will be LOW while the phase shift θ is taking its effect. Therefore, by integrating the V_{s2}:

$$V_{LPF} = \begin{cases} \frac{V_R}{2}\left(1 - \frac{\theta}{180°}\right); & 0° < \theta < 180° \\ \frac{V_R}{2}\left(\frac{\theta}{180°} - 1\right); & 180° < \theta < 360° \end{cases} \tag{2.12}$$

which is piecewise function of θ. As V_{LPF} is inversely proportional to θ on the interval $[0°, 180°]$ and directly proportional to θ on the interval $[180°, 360°]$. To fully linearize V_{LPF}, they needed a circuitry to detect if the θ is greater / less than $180°$ to decide wither to invert V_{LPF} or to keep it. To do that, they utilized V_{B2} and V_2 as they compared each one

to Zero and XNORed their square wave outputs. Note that, $V_2 = V_{B2} * \sin(\theta)$. Thus, if the outputs of the two comparators are equal, then the $\sin(\theta)$ is positive as it did not alter the sign of V_{B2}, thus, $\theta < 180°$ and vice versa. The output of the XNOR is then utilized as to control the third SPDT switch which switches between a non-inverted and an inverted version of V_{LPF}. The output of the third switch, V_o, is then linear on the full circle range. The practical error of the circuit itself was $< 0.1\%$ and the practical error of the overall circuit was $< 0.85\%$. It can be seen that the error of [37] is better than that of [35] , yet it used more comparators and switches than the former method. On the other hand, they eliminated the need of one-shot circuit.

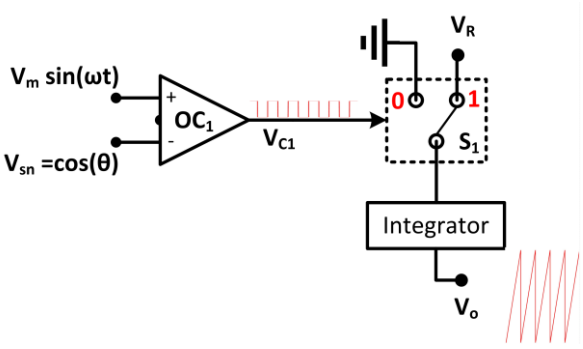

Figure 2.4. The proposed convertor in [38]

In [38], the main idea of the author was to linearize $\cos(\theta)$. To do that, they assumed that the GMR sensor is supplied by a constant DC power sources so that the output would be in the form of $V_{sn} = \cos(\theta)$. V_{sn} is then compared to a reference signal $\sin(\omega t)$ through a comparator. Thus, the comparator's output will be:

$$v_{c1} = \begin{cases} HIGH;\ sin(\omega t) > cos(\theta) \\ LOW\ ;\ sin(\omega t) < cos(\theta) \end{cases} \quad (2.13)$$

Thus, the duration of the output of the comparator, V_{c1}, depend directly on the angle of interest, θ. Like the procedure mentioned in [35], $V_{c1}$is utilized to control an SPDT switch that switches between Ground or V_R, which is then integrated to find an output that is linearly proportional to the angle of interest, θ. Yet, the difference here is that the output's slope will change, depending on the angle of operation. For example, the output will have a positive slope when $0° < \theta < 180°$. Then the slope will be negative in the range of $180° < \theta < 360°$. Thus, there would be ambiguity of knowing wither the angle of interest, θ, is within the first half or the second half of the operation scale. Therefore, on one hand, the proposed method is much simpler in implementation than that of [35], yet, it can only detect the angular position in half of the range of operation only. The simulation error was found to be $< 0.3°$ in the full range of operation, while it was $< 0.03°$ when $5° < \theta < 175°$. That's due to the high error found around $\theta = 0°$ and $\theta = 180°$ were the cosine have its lowest sensitivity and due to the mismatch between the two compared signals, V_{sn} and Vm. Practically, the error was $< 0.3°$ within the same range. The proposed method also goes under a risky assumption that the change of the angle of interest is negligible under one cycle of the reference sinusoidal signal. Thus, in order to decrease this risk, the frequency of oscillation of the reference signal should be increased. Yet, it is bounded by the slew rate of the electronics used within the proposed method.

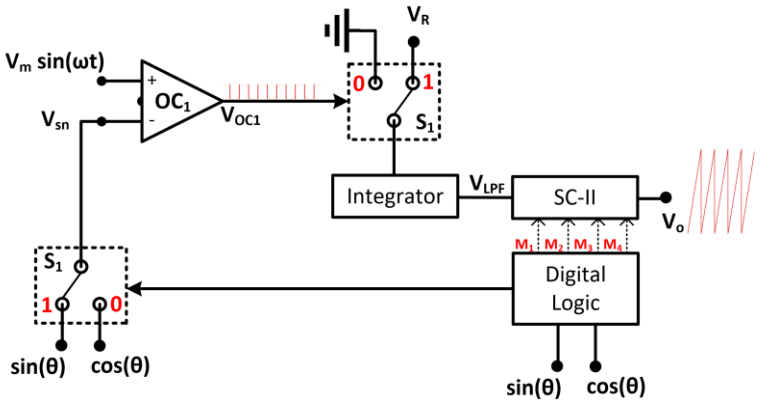

Figure 2.5. The proposed convertor in [39], [40]

The work of [39] and [40] was a built upon the findings of [38]. As they first solved the issue of range of operation, then, the improved the overall sensitivity of the system by utilizing both quadrature outputs of the GMR sensor instead of only utilizing the cosine. The circuitry proposed above is the same, but, V_{sn} is now an output of an SPDT switch which chooses between either $\sin(\theta)$ or $\cos(\theta)$. Depending on a logic that will be evident later. Either ways, the output of the integrator, V_{LPF}, will still be suffering from the ambiguity. If $\cos(\theta)$ was chosen, the output of V_{LPF} will be as discussed in [38]. Yet, if the $\sin(\theta)$ was chosen, the output will be:

$$V_{LPF} = \begin{cases} \frac{V_R}{2} - \frac{V_R}{180°}\theta; & 0° < \theta < 90° \\ \frac{V_R}{180°}\theta - \frac{V_R}{2}; & 90° < \theta < 270° \\ 2.5V_R - \frac{V_R}{180°}\theta; & 270° < \theta < 360° \end{cases} \quad (2.14)$$

To solve that, they proposed a simple logic design that depends on the values of $\sin(\theta)$ and $\cos(\theta)$ to detect the quadrant of operation. First, to detect if θ is greater / less

than 180°, $\sin(\theta)$ was compared to ground. Then, to detect the four quadrants, $\pm\sin(\theta)$ and $\pm\cos(\theta)$ can be compared together. After a rough detection at which section the angle lies, adequate signal correction takes place by utilizing a number of operational amplifiers. Now, in order to choose the best signal among sine and cosine in terms of sensitivity, the following was done.

$$V_{sn} = max\left(\frac{d}{d\theta}sin(\theta), \frac{d}{d\theta}cos(\theta)\right) \tag{2.15}$$

Thus, it can be proven, that cosine will be chosen at intervals of $[45°; 135°]$ and $[225°; 315°]$ or simply when $-\frac{\sqrt{2}}{2} < \cos(\theta) < \frac{\sqrt{2}}{2}$ and sine will be chosen otherwise. Although the proposed method had far more components than the prior work, yet, it had far lower error. The proposed method was applied practically and had a maximum error of 0.08%. And more importantly, it has the full range of operation unlike the former work.

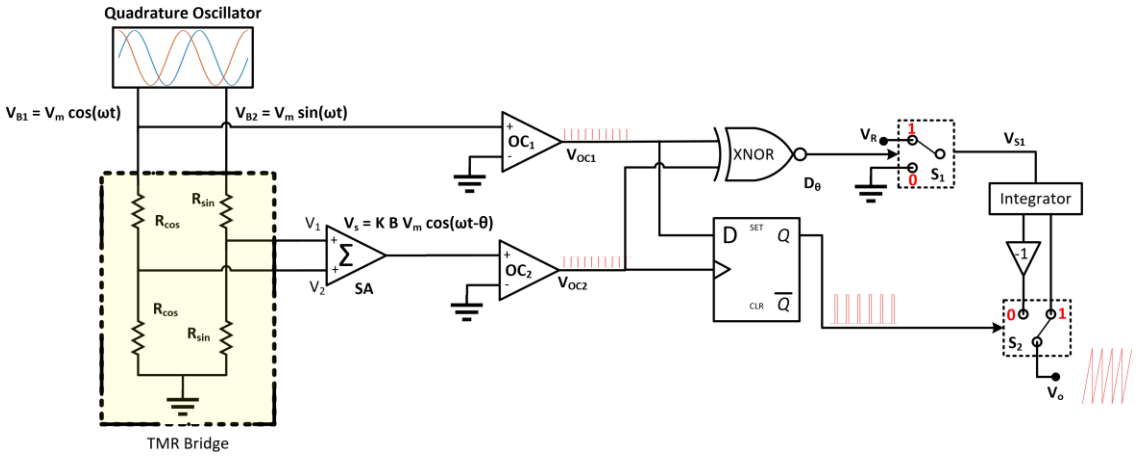

Figure 2.6. The proposed convertor in [13]

The idea proposed in [13] is based on the idea proposed earlier in [35], [36]. As the TMR sensor is powered through the same quadrature oscillator, and having its modulated outputs summed to produce $V_s = \cos(\omega t - \theta)$. Both V_s and $\cos(\omega t)$ are inputted into two comparators to produce two square wave signals that are phase shifted apart by θ, V_{oc1} and V_{oc2} respectively. Then they connect V_{oc1} to the D terminal of a positively triggered flip flop and V_{oc2} to its clock. Thus, the output of the flip flop, Q, will be:

$$Q = \begin{cases} LOW; 0° < \theta < 180° \\ HIGH; 180° < \theta < 360° \end{cases} \quad (2.16)$$

Also, V_{oc1} and V_{oc2} are XNORed to output D_θ. D_θ will always be HIGH while both signals are of the same value. Thus, it will be LOW only for the time period of their phase shift, when they are not of the same value. The period of the phase shift is related to the angle of interest, θ. Thus, as previously discussed, integrating such signal will give two piece-wise linear functions with $\pm$ slopes mirrored at $180°$. There, they utilized the signal Q which detects angle $180°$ and inverts the negative slope accordingly. By that, they have accomplished linearity for the full range of operation with much less components than the previously discussed works. According to the simulations and emulations, the proposed circuit has a maximum error $< 0.13\%$. While peaking at 0.92% error at practical implementation of the whole instrumentation system.

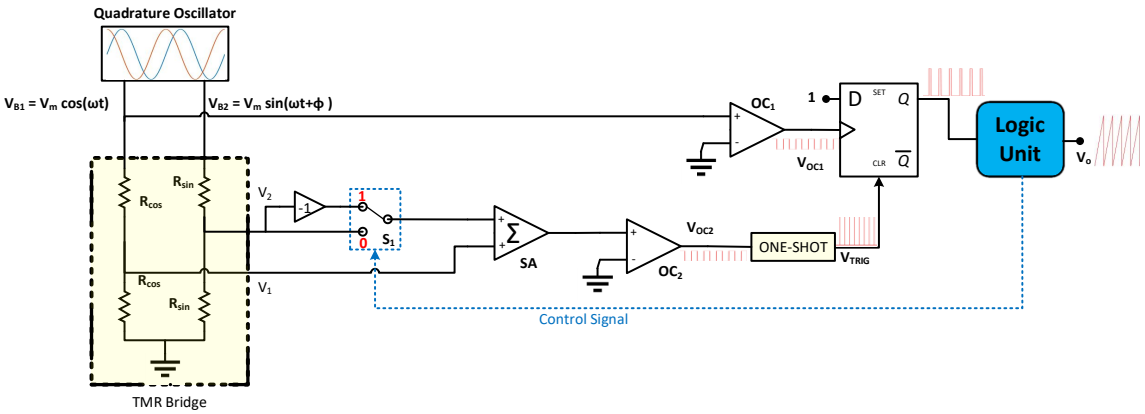

Figure 2.7. The proposed convertor in [14]

In [14], the authors presented one of the issues that is usually associated with the proposed methods in [35], [36] which is having an imbalance phase shift, ϕ, within the quadrature oscillator powering the TMR sensor and how would such small shift give rise to high errors within the measured output angle as the measurement at the end will be proportional to $(\phi + \theta)$ instead of θ only. They modeled that shift to be:

$$V_{B2} = sin(\omega t + \phi) \tag{2.17}$$

Thus, the modulated outputs would be:

$$V_1 = cos(\omega t)\, cos(\theta) \tag{2.18}$$

$$vV_2 = sin(\omega t + \phi)\, sin(\theta) \tag{2.19}$$

Within this paper, they proposed a scheme to solve such issue. Now, instead of having one summation between the modulated signals of the TMR directly, they proposed to have two versions of summations depending on a control signal, such that the output of the summing amplifier would be:

$$V_{SA} = \begin{cases} cos\big((\omega t + \phi) + \theta\big)\,; Control\ Signal = HIGH \\ cos\big((\omega t + \phi) - \theta\big)\,; Control\ Signal = LOW \end{cases} \quad (2.20)$$

This is done by choosing between an inverted and a non-inverted version of $\sin(\omega t + \phi)\sin(\theta)$ to be summed with $\cos(\omega t)\cos(\theta)$. Next, after having either possible summation outputs, they will be processed as proposed in the former work through comparators, a D flip flop and integration to produce two outputs that are linearly proportional to $(\phi + \theta)$ and $(\phi - \theta)$. Thus, by taking the difference between them and dividing by two we get the output signal proportional to θ only:

$$V_o = \frac{(\phi + \theta) - (\phi - \theta)}{2} = \frac{2\theta}{2} = \theta \quad (2.21)$$

It was found through simulations that the error of the proposed scheme was 0.15% independent of the amount of phase imbalance ϕ as well as 0.5% error practically, which is even better than the former work performance.

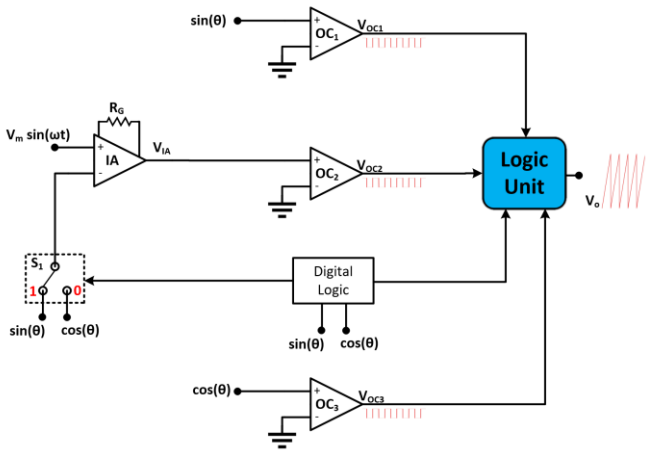

Figure 2.8. The proposed convertor in [15]

The latest work proposed by the authors in [15] utilizes the merits of [39], [40] of choosing between the two outputs of the TMR depending on maximum sensitivity combined with a new phase detection technique to propose a new MR converter. They proposed that the sensor would be powered through a DC source, V_{DC} and that only one the outputs of the sensors, $V_{DC}\cos(\theta)$ and $V_{DC}\sin(\theta)$, will be chosen from to be V_s, depending on the aforementioned logic, to be subtracted from $V_r = V_m \sin(\omega t)$ through an Instrumentation Amplifier (IA). Such that, the output of the IA would be V_r with a DC shift depending on θ:

$$V_{IA} = V_m\, sin(\omega t) - V_s \tag{2.22}$$

V_{IA} is then inputted to a comparator, which will output a signal that is proportional to the amount of DC shift introduced, which in turn depend on the angle of interest, θ. The output can then be integrated as discussed in former works to produce a piece-wise linear function that is then rectified through the aforementioned logic in previous works. The proposed techniques have a maximum simulation error of 0.014% and 0.12% practically, which is far superior to the previous works, while eliminating the need of quadrature oscillators, monostable multivibrators and flip-flops.

In conclusion, few MR sinusoidal to angle converters were proposed in literature. They varied in complexity and performance, yet, all of them were open loop based. Which in fact are dynamically faster than closed loop converters but are more vulnerable towards noise and instabilities found in the environment of operation. Towards filling that gap, the next chapter proposes a novel closed loop method based on the well-known Phase Locked Loop technique.

CHAPTER 3: PROPOSED CLOSED LOOP CONVERTER

3.1 Phase Locked Loop (PLL) based converters in literature

3.1.1 Introduction about PLLs

Phase locked loops are one of the well-known closed loop control techniques that are used in various fields that requires synchronization between two sources such as in communication systems and many more. As the name suggests, PLL works toward adjusting the phase of one source to match the other. Once that happens, the loop is locked. PLLs in general consists of three main blocks, Phase Detector (PD), loop filter and Voltage Controlled Oscillator (VCO) as seen in Figure 3.1.

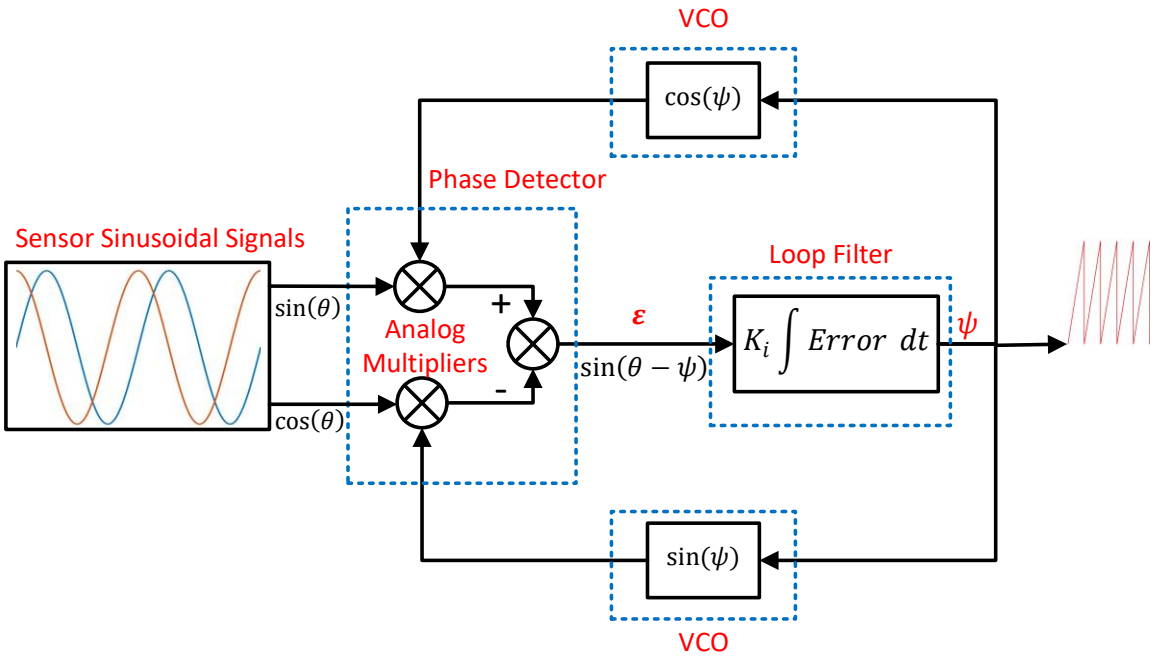

Figure 3.1. Classical PLL Block Diagram

The main idea is to adjust the phase of the VCO to match that of the reference signal. The Phase detector is a mechanism that computes the difference between the two sources' phases; usually called the error signal "ε". The loop filter is usually an integrator or a PI controller that works toward driving the error signal to zero and controlling the VCO. The VCO, is an oscillator that produces a sinusoidal wave that has its frequency / phase controlled through an input voltage. VCOs' frequency of oscillation may have a linear or a non-linear relationship with the input voltage, but, it should be a monotonic relationship in either cases. The output of the VCO is then utilized within the PD stage to compute the error signal, and hence the loop is closed. Many research works was done towards enhancing the PLL mechanism by lowering its cost and complexity as in [5], [41], [42], [43] and [44] as well as improving its dynamic response as in [41], [43],[44] and [45]. It is worth noting that most of the enhanced PLL methods presented in the literature do usually target PLL converters designed for Resolvers. Thus, the aim is usually to find solutions that integrates the modulation/demodulation process that takes place in resolver based systems into their proposed methods. Nevertheless, these enhanced PLL methods can also be applied to other sinusoidal angular position encoders including TMR sensors.

3.1.2 Literature Review of Proposed enhancements to PLL converters

Complexity of the classical PLL method may be decreased by enhancing any of the three individual blocks of the PLL stages. Towards lowering the complexity of the PLL feedback generators; VCO in classical PLLs, [41] suggested to replace the classical VCO by a simple all analog Triangle-Sine conversion technique, which is done through Transdiodes; by utilizing their nonlinear I-V characteristics. Also, [5] lowered the

complexity of the signal generation, PD and demodulation stages, by replacing the classical synchronous demodulators by full-wave / half-wave rectifiers to rectify the modulated signals. These signals are then inputted to the PD stage. Hence, only single-quadrant multipliers will be needed as opposed to the four quadrant expensive multipliers needed within the classical PLL method. For the feedback sinusoidal signal generation, it was proposed to approximate them through a ratiometric polynomial formula invented in the 7th century by the Indian mathematician Bhaskara:

$$\sin(\psi) = \frac{1.0468\psi - 0.4278\psi^2}{1 - 0.2618\psi} \qquad 3.1)$$

The approximation technique has a maximum absolute error of $Error_\theta = 0.16\%$. The proposed ratiometric polynomial technique can be realized through simple network of Operational Amplifiers circuitry. Thus, the need for VCO was eliminated and the complexity was lowered. In [42] however, the feedback signal generation complexity was lowered by utilizing the resolver's excitation signals. It was proposed to compare the estimated angle ψ to the excitation angle ωt. When they are equal, two sample and hold circuits are triggered to take samples of the excitation signals $\sin(\omega t)$ and $\cos(\omega t)$; which in theory will also be equal to $\sin(\psi)$ and $\cos(\psi)$ respectively. The output of the two sample and hold circuits will be used to as the feedback signals for the PD to operate. In [43] and [44], the author proposed to excite the resolver through pulse excitation signal; rather than sinusoidal signal, and use that signal to demodulate and sample the resolver's output signals. This will reduce the complexity of the generation of the excitation signals; as any microcontroller would be able to produce such signal easily, as opposed to the classical sinusoidal excitation signal used.

Towards improving the dynamics and accuracy of the classical PLL based converter, [41] suggested to feedforward a scaled version of the error signal ε and add it to the estimated angle ψ. This will in turn adjust the initial conditions of the PLL to a much near state to the true angle almost instantaneously, thus, the dynamics of the system is improved. [43],[44] and [45] proposed to integrate an open loop coarse angle estimator with the classical PLL as an initial condition estimator. The open loop coarse angle estimator divides the angular range $[0° - 360°]$ into 8 equal sections and estimates the true angle's current section by simple comparison relations between the input sinusoidal signals. Afterwards, the mid angle of the estimated section will be added to the output of the PLL as an initial condition; Which enhances the dynamics of the system greatly.

In conclusion, research work in this field usually tends to enhance the PLL based converters by reducing their complexity and hence their cost, in addition to improving their dynamic performance. The next section will discuss the proposed novel method which in turn will lower the classical PLL's complexity and cost.

3.2 Proposed Method

3.2.1 Problem Statement

It can be noticed that a common expensive component for all PLL based converters proposed is the analogue multiplier, which has a crucial role within the implementation of the Phase-Detector (PD) stage of the PLL. As it multiplies the sinusoidal outputs of the TMR sensor with the feedback sinusoidal signals. Having PLLs operating without the need of multipliers is a great plus to the complexity and the price of the PLL based converter. In

the light of the above, a novel method is proposed to eliminate the need for analog multipliers by emulating the multiplication process within the sensor itself. This is done through exploiting the power supplies of the TMR sensor by feeding back the feedback sinusoidal signals $\sin(\psi)$ and $\cos(\psi)$ through them. As mentioned earlier, the TMR technology is constructed upon the voltage division principle of the supply voltage between the magnetoresistive elements. Thus, the outputs of the voltage dividers are inherently multiplied by the supply voltage as seen earlier in (2.3) and (2.4). Therefore, having the supply of the "Sine" and "Cosine" branches of the TMR sensor to be proportional to $\cos(\psi)$ and $\sin(\psi)$ respectively, the output voltage of the bridges would be proportional to:

$$V_{Sin} = \cos(\psi)\left(\sin(\theta) + \frac{1}{2} + V_{Offset}\right) \tag{3.2}$$

$$V_{Cos} = \sin(\psi)\left(\cos(\theta) + \frac{1}{2} + V_{Offset}\right) \tag{3.3}$$

Thus, by removing the additive component, for example through a simple Instrumentation Amplifier circuitry, the outputs will be ready to be subtracted to get the error signal ε as seen in Figure 3.2.

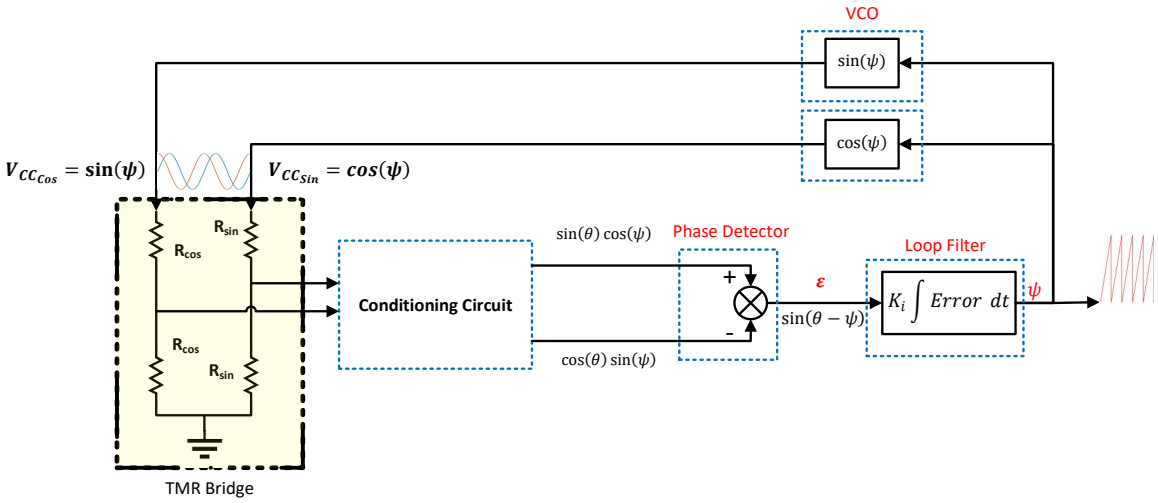

Figure 3.2. Proposed enhanced PLL converter

3.2.2 Modified Imbalance Correction Schemes

The sensor signals may commonly present imbalances in their Amplitudes (i.e., mismatch between the peak-to-peak amplitudes of the two signals), DC shift (i.e,, the two signals have different DC components) or Phase shift (i.e., the phase shift between the two signals is not 90°) as seen earlier in (1.7) and (1.8). Once the imbalance is detected and quantified, simple corrective actions may be taken. Solutions for amplitude imbalance may include multiplying one of the signals by a gain to match it to the other. DC shift imbalance may be corrected by shifting signals up/down to null any DC offset and DC offset imbalance. Yet for the case of phase shift imbalance, some higher mathematical trigonometric identities are used to resolve them. Assuming for example that the cosine signal is used as reference and the sensor produces signals proportional to $cos(\theta)$ and $sin(\theta + \phi)$; where ϕ is the phase imbalance, the sine output can be expressed as:

$$\sin(\theta + \phi) = \sin(\theta)\cos(\phi) + \cos(\theta)\sin(\phi) \tag{3.4}$$

Thus, to extract the balanced sine, the following operation is usually done:

$$\sin(\theta) = \frac{\sin(\theta + \phi) - \cos(\theta)\sin(\phi)}{\cos(\phi)} \tag{3.5}$$

where $\sin(\phi)$ and $\cos(\phi)$ are constants that can be generated once ϕ is known, and $\sin(\theta + \phi)$, $\cos(\theta)$ are the original sinusoidal signals.

Now since the signals will be inherently multiplied by the feedback, and no direct path is available to correct the raw signals before the multiplication as they were usually done. Consequently, new correction techniques are needed to correct the DC and phase shift imbalance; amplitude imbalance correction is still applicable. Now, assuming that the raw signal was in the form of:

$$V_{Sin} = V_{CC_{Sin}}\left(A(1 + \alpha) \cdot \sin(\theta + \phi) + V_{Offset_{Sin}}\right) \tag{3.6}$$

then, after multiplication, the signal will be:

$$V_{Sin} = A(1 + \alpha) \cdot \cos(\psi) \cdot \sin(\theta + \phi) + V_{Offset_{Sin}} \cdot \cos(\psi) \tag{3.7}$$

To remove the DC shift $V_{Offset_{Sin}}$, it should first be multiplied by the feedback signal $\cos(\psi)$ then subtracted from the multiplied signal to be:

$$V_{Sin} = A(1 + \alpha) \cdot \cos(\psi) \cdot \sin(\theta + \phi) \tag{3.8}$$

then the amplitude imbalance can be removed easily through simple division to be:

$$V_{Sin} = A.\cos(\psi) \cdot \sin(\theta + \phi) \tag{3.9}$$

Now for the phase imbalance, a novel method is proposed to apply the correction. It is proposed to exploit the TMR's supply once more imbue the phase imbalance ϕ within one of the feedback signals. For instance, in the case above; $\sin(\theta + \phi)$, the phase imbalance

will be introduced also into the Sine feedback; shown in Figure 3.3, to be:

$$\sin(\psi + \phi) \tag{3.10}$$

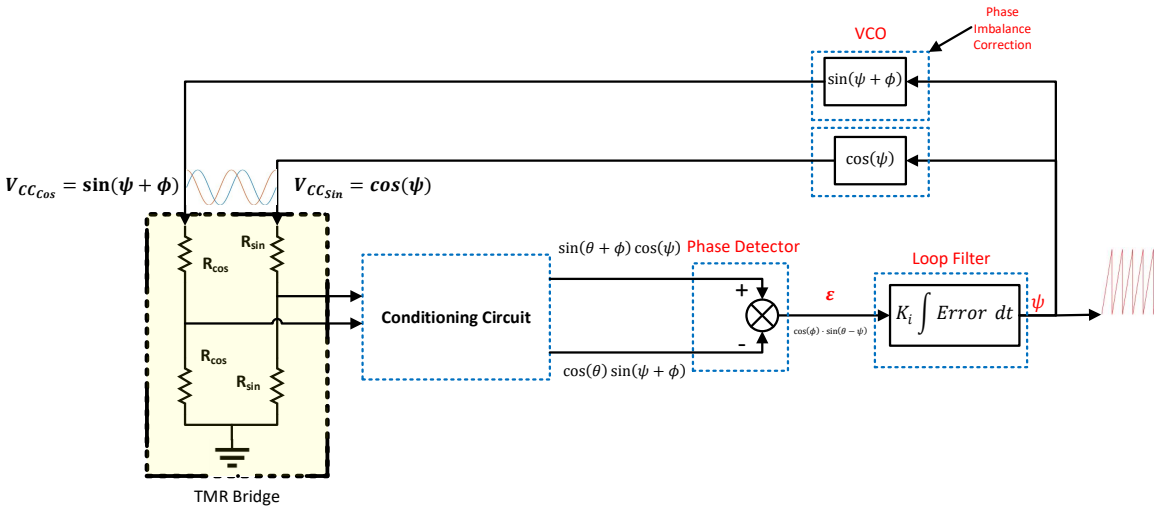

Figure 3.3. Proposed converter incorporating the proposed phase imbalance correction technique

that way, the error signal will be as follows:

$$\begin{aligned}
\varepsilon = {} & cos(\psi) \cdot sin(\theta + \phi) - cos(\theta) \cdot sin(\psi + \phi) \\
\varepsilon = {} & cos(\psi) \cdot [sin(\theta) \cdot cos(\phi) + sin(\phi)\, cos(\theta)] \\
& - cos(\theta) \cdot [sin(\psi) \cdot cos(\phi) + sin(\phi)\, cos(\psi)] \\
\varepsilon = {} & cos(\psi)\, sin(\theta)\, cos(\phi) + \cancel{cos(\psi)\, sin(\phi)\, cos(\theta)} \\
& - cos(\theta)\, sin(\psi)\, cos(\phi) - \cancel{cos(\theta)\, sin(\phi)\, cos(\psi)}
\end{aligned} \tag{3.11}$$

$$\varepsilon = cos(\phi) \cdot [sin(\theta)\, cos(\psi) - sin(\psi)\, cos(\theta)]$$

$$\varepsilon = cos(\phi) \cdot sin(\theta - \psi)$$

which is the error signal obtained with classical PLL with an addition constant gain which can be compensated in the loop filtering gain stage. This method has a clear advantage over the ordinary phase compensation technique, as the former only works fine while assuming that the input signals are free of amplitude and dc imbalance, as it is directly relying on them. In fact, the former phase correction technique would yield to more error if the input sinusoidal signals are not balanced as will be discussed in the following chapter. On the other hand, the proposed method is clearly independent of the input sinusoidal signals, which is a great plus.

3.3 Simulations

In practice, many factors affect the instrumentation performance, such as noise, interference, loading effects, etc. On the other hand, the simulation environment is very controlled in that sense. Hence, in order to have a ceiling of the expectations of the proposed methods, they were first implemented within a controlled environment of simulation via MATLAB Simulink. The simulations incorporate different scenarios of amplitude, DC offset and phase imbalances. The sensor sinusoidal amplitude was assumed to be 7.5V and was run at 1 rev/sec at perfect imbalance free conditions. The PLL filter gain was set to 1000 and simulation time step was set to 7.5us. Thus, the expected steady state error would be $Error_\theta = \psi - \theta = \frac{360^\circ}{7.5 \times 1000} = 0.048^\circ$. The perfect imbalance free simulation result is shown at the top of Figure 3.4. As expected from the dynamics of PLLs,

the error was steady around $0.048°$, with 0 Peak-Peak (PP) error. After that, four different combinations of imbalances were chosen and tested. The chosen imbalances; illustrated in Table 3.1 and Figure 3.4 , reflect realistic imbalances and are not exaggerated.

Table 3.1. Imbalance Simulation Scenarios

	α	DC_{Sin}	DC_{Cos}	ϕ
Scenario 1.1	0.001	0.05	0	$1°$
Scenario 1.2	-0.001	0.05	0.05	$1.5°$
Scenario 1.3	-0.001	0	-0.05	$2°$
Scenario 1.4	-0.001	0	-0.05	$0°$

It can be seen from Figure 3.4, that the tested imbalances introduce a PP $Error_\theta$ in the range of $1° - 2.5°$.

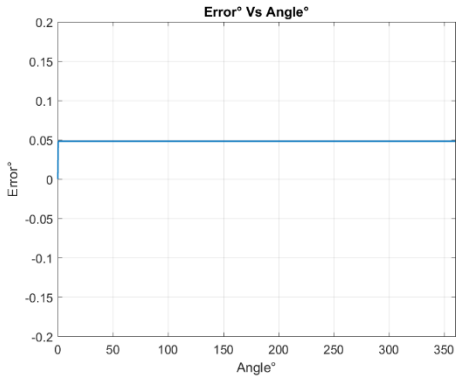

(a)

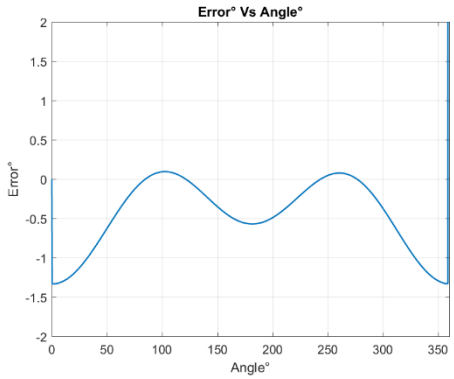

(b)

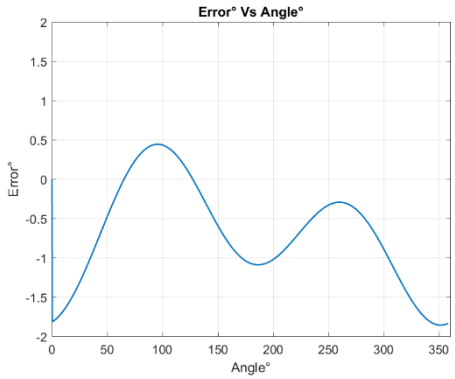

(c)

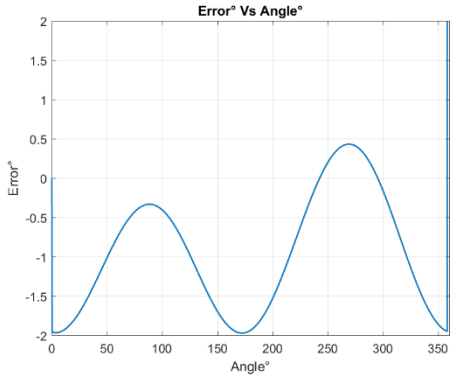

(d)

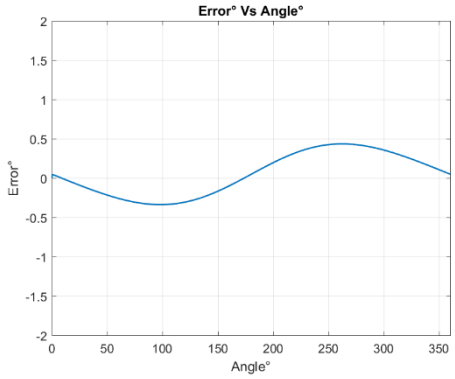

(e)

Figure 3.4. Perfect (a) & imbalance simulation scenarios (1.1-1.4) in order from left to right (b-e)

Utilizing the same simulation, the proposed DC shift and phase imbalance correction techniques were tested. Figure 3.5 show their $Error_\theta$ waveform after correction. The Amplitude imbalance was intentionally not corrected for two reasons. First, if all imbalances were corrected, all results will be an exact replica of the imbalance free figure. Second, it was done to show that; in general, by compensating for some of the errors, the total $Error_\theta$ may decrease, but to get 0 PP $Error_\theta$, therefore, all imbalances should be addressed. The results show that the proposed imbalance correction techniques proposed work in simulation. Also, it shows that the PP contribution of the amplitude imbalance is expected to be around 0.06° if the amplitude imbalance was 1% only.

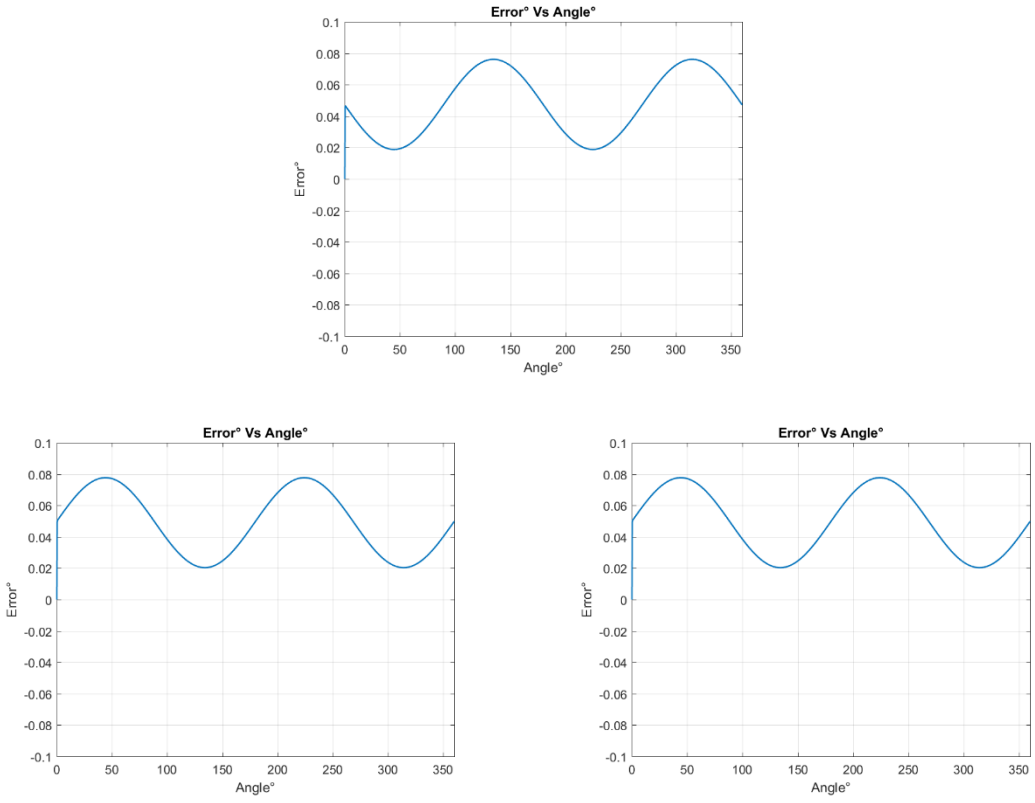

Figure 3.5. Proposed phase imbalance correction technique simulation results of scenarios (1.1-1.3) in order from left to right

It is important to note that in addition to amplitude, DC offset and phase imbalances, the sensors may present other equally important imperfections. For the MR sensor, relatively far or short distance between the permanent magnet and TMR sensor results in harmonics (particularly 3rd) in the sensor signals. Tests were carried out by adding 6 different combinations of 3rd harmonic $\sin(3 \cdot \theta)$ and $\cos(3 \cdot \theta)$ signals; of relative amplitudes A_3 and B_3 respectively, to the original sinusoidal signals in addition to the aforementioned imbalances; the combinations and results are shown in Table 3.2 and Figure 3.6 respectively.

Table 3.2. Harmonic Distortion Simulation Scenarios

	A_3	B_3	$\alpha/DC_{Sin}/\phi$
Scenario 2.1	1%	0%	Perfect $(0/0/0°)$
Scenario 2.2	0%	1%	Perfect
Scenario 2.3	1%	1%	Perfect
Scenario 2.4	1%	0.25%	Perfect
Scenario 2.5	0%	1%	$0/0.01/0.5°$
Scenario 2.6	0%	1%	$0/-0.03/-0.2°$

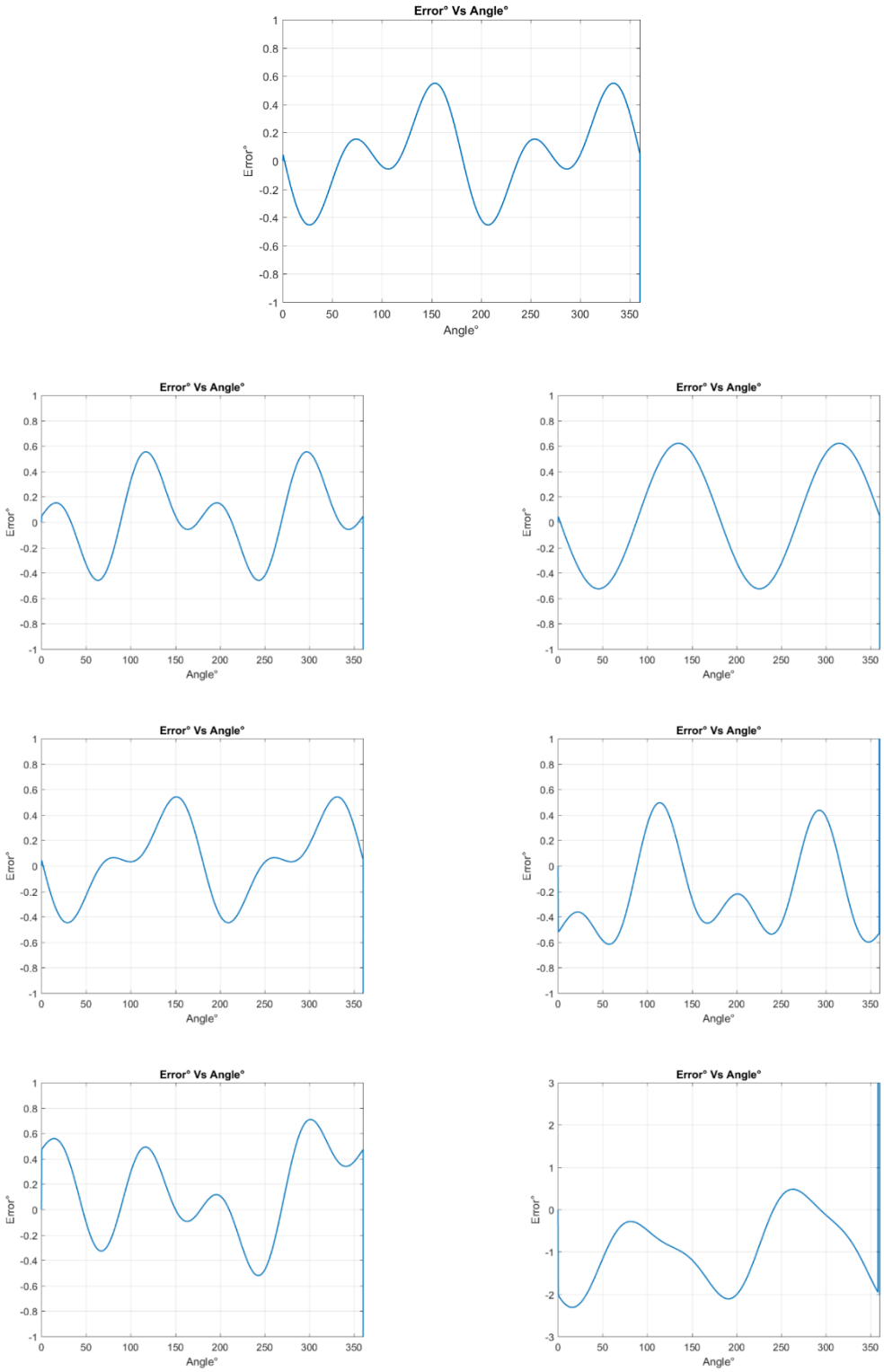

Figure 3.6. Harmonic distortion simulation scenarios (2.1-2.6) in order from left to right

It can be seen from Figure 3.6 that the slightest interference of harmonics (1%) may have a great impact on the results, as it may contribute with a PP $Error_\theta$ of 1°. More interestingly, Harmonics errors can have different characteristic from the other imbalance errors, and thus can be distinguished if present. For example, the number of peaks in the $Error_\theta$ waveform. In the first three imbalance types, for any combination, there is a maximum of 2 peaks per revolution. Yet, for the harmonic imbalance, the $Error_\theta$ waveform usually has 4 peaks, except for the case of having a balanced interference on both sine and cosine as in Scenario 2.3, only in that case the $Error_\theta$ waveform would have 2 peaks only. The following mathematical proof proves these claims.

Assuming the general case of having both Sine and Cosine having a 3rd harmonic distortion with amplitudes A_3 and B_3 respectively. Thus, the output of the PD stage will be in the form of:

$$\begin{aligned}
\varepsilon = & \left(\underbrace{\sin(\theta)} + A_3 \cdot \sin(3 \cdot \theta)\right) \times \underbrace{\cos(\psi)} \\
& - \left(\underbrace{\cos(\theta)} + B_3 \cdot \cos(3 \cdot \theta)\right) \times \underbrace{\sin(\psi)} \\
\varepsilon = & \left(\underbrace{\sin(\theta)\cos(\psi) - \cos(\theta)\sin(\psi)}\right) \\
& + A_3 \cdot \sin(3 \cdot \theta)\cos(\psi) + B_3 \cdot \cos(3 \cdot \theta)\sin(\psi) \\
\varepsilon = & \sin(\theta - \psi) + A_3 \cdot \sin(3 \cdot \theta)\cos(\psi) + B_3 \cdot \cos(3 \cdot \theta)\sin(\psi) \\
\varepsilon \approx & (\theta - \psi) + A_3 \cdot \sin(3 \cdot \theta)\cos(\psi) + B_3 \cdot \cos(3 \cdot \theta)\sin(\psi)
\end{aligned} \tag{3.12}$$

Then, after integrating the error signal ε, it will be driven to Zero, and thus, the deviation of the estimated angle ψ from the real angle θ will be:

$$Error_\theta = A_3 \cdot \sin(3 \cdot \psi)\cos(\psi) + B_3 \cdot \cos(3 \cdot \psi)\sin(\psi) \tag{3.13}$$

"B_3" can be assumed to be equal to "A_3" plus a constant "C_3", $B_3 = A_3 + C_3$. Thus, equation (3.13) can be re-written as:

$$\begin{aligned} Error_\theta &= \underbrace{\left(A_3 \cdot \sin(3 \cdot \psi)\cos(\psi) - A_3 \cdot \cos(3 \cdot \psi)\sin(\psi)\right)}_{} \\ &\quad - C_3 \cdot \cos(3 \cdot \psi)\sin(\psi) \\ Error_\theta &= A_3 \cdot \sin(2 \cdot \psi) - C_3 \cdot \cos(3 \cdot \psi)\sin(\psi) \end{aligned} \tag{3.14}$$

The number of peaks of the deviation signal and their places can be found by derivating it with respect to ψ it and equating the result to Zero and finding the roots as shown below:

$$\frac{dError_\theta}{d\psi} = 2A_3 \cdot \cos(2 \cdot \psi) - C_3 \cdot \left[-\overbrace{3 \cdot \underbrace{\sin(3 \cdot \psi)\sin(\psi)}}} + \underbrace{\cos(3 \cdot \psi)\cos(\psi)}\right]$$

$$\frac{dError_\theta}{d\psi} = 2A_3 \cdot \cos(2 \cdot \psi) - C_3 \cdot \left[\underbrace{\cos(4 \cdot \psi)} - \overbrace{2 \cdot \sin(3 \cdot \psi)\sin(\psi)}\right]$$

$$\frac{dError_\theta}{d\psi} = 2A_3 \cdot \cos(2 \cdot \psi) - C_3 \cdot \left[\cos(4 \cdot \psi) - 2 \cdot \left(-\frac{\cos(4 \cdot \psi) + \cos(2 \cdot \psi)}{2}\right)\right]$$

$$\frac{dError_\theta}{d\psi} = \underbrace{2A_3 \cdot \cos(2 \cdot \psi)} - C_3 \cdot \left[2 \cdot \cos(4 \cdot \psi) \underbrace{- \cos(2 \cdot \psi)}\right] \tag{3.15}$$

$$\frac{dError_\theta}{d\psi} = \underbrace{(2A_3 + C_3) \cdot \cos(2 \cdot \psi)} - 2C_3 \cdot \cos(4 \cdot \psi) = 0$$

$$\frac{dError_\theta}{d\psi} = \cos(4 \cdot \psi) - \left(\frac{2A_3 + C_3}{2C_3}\right)\cos(2 \cdot \psi) = 0$$

$$\frac{dError_\theta}{d\psi} = \frac{1 + \cos(4 \cdot \psi)}{2} - \left(\frac{2A_3 + C_3}{4C_3}\right)\cos(2 \cdot \psi) = \frac{1}{2}$$

$$\frac{dError_\theta}{d\psi} = \cos^2(2 \cdot \psi) - \left(\frac{2A_3 + C_3}{4C_3}\right)\cos(2 \cdot \psi) - \frac{1}{2} = 0$$

$$\rightarrow u = \cos(2 \cdot \psi) \tag{3.16}$$

$$\frac{dError_\theta}{d\psi} = u^2 - \left(\frac{2A_3 + C_3}{4C_3}\right) - \frac{1}{2} = 0; \tag{3.17}$$

The roots of the equation (3.17) can then be found through the quadratic formula to be:

$$u = \frac{\left(\frac{2A_3 + C_3}{4C_3}\right) \pm \sqrt{\left(\frac{2A_3 + C_3}{4C_3}\right)^2 + 2}}{2} \tag{3.18}$$

$$\psi = \frac{1}{2} \cdot \cos^{-1}(u) \tag{3.19}$$

Equation (3.18) may always result in two unique solutions for "u", as the expression under the square root is always positive. Which in turn, will result in four unique ψ roots; (3.19) for each solution of "u", to have a total of 8 roots. Four of which are local maximums (Peaks) and the rest are local minimums (crests), which proves the proposed claim of having four peaks in the presence of unbalanced harmonic interference.

In the case of the absence of one side of the Sine or Cosine harmonic interferences; "C_3" will be reduced to:

$$C_3 = \begin{cases} B_3; A_3 = 0 \\ -A_3; B_3 = 0 \end{cases} \tag{3.20}$$

Hence, "u" will be reduced to:

$$u = \begin{cases} +\dfrac{1 \pm \sqrt{33}}{8}; A_3 = 0 \\ -\dfrac{1 \pm \sqrt{33}}{8}; B_3 = 0 \end{cases} \tag{3.21}$$

In the case of having balanced interference; i.e. 3rd harmonic present at both sine and cosine terminals with equal amplitude A_3, (3.14) will reduce to:

$$Error_\theta = A_3 \cdot \sin(3 \cdot \psi)\cos(\psi) - A_3 \cdot \cos(3 \cdot \psi)\sin(\psi) \tag{3.22}$$

$$Error_\theta = A_3 \cdot \sin(2 \cdot \psi) = 0$$

Which will have four roots, two of which are peaks and the other two are crests. Which proves the second claim.

It is worth noting that this characteristic only persists when the contributing error of the harmonic is relatively higher than other aforementioned sources of error. Else, the peaks of the harmonic imbalance $Error_\theta$ waveform would be overshadowed by them; as seen in Scenario 2.6, and hence, they will not be visible until the other sources of error were corrected for.

CHAPTER 4: PRACTICAL IMPLEMENTATION, RESULTS AND DISCUSSION

4.1 Practical Setup

Towards testing the proposed methods, a practical setup was built. The setup consists of a DC motor connected to a gear to step down its speed, a permanent magnet, and a TMR sensor which is placed on a PCP. The PCB is fixed through four screws at its corners, the screws are relatively long to give a freedom to test with different displacements between the PM and the TMR sensor with different orientations. On the other side of the motor, an optical pulse encoder is integrated to simultaneously report the angle of rotation for benchmark purposes. The motor setup is shown in Figure 4.1 and Figure 4.2.

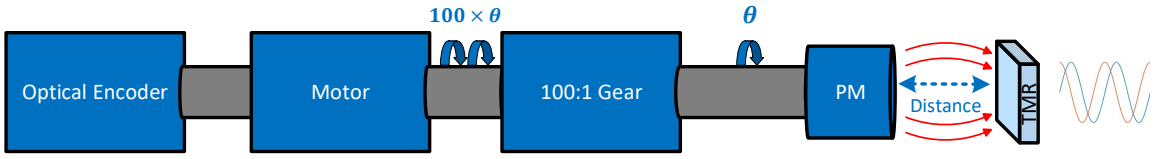

Figure 4.1. DC motor setup block diagram

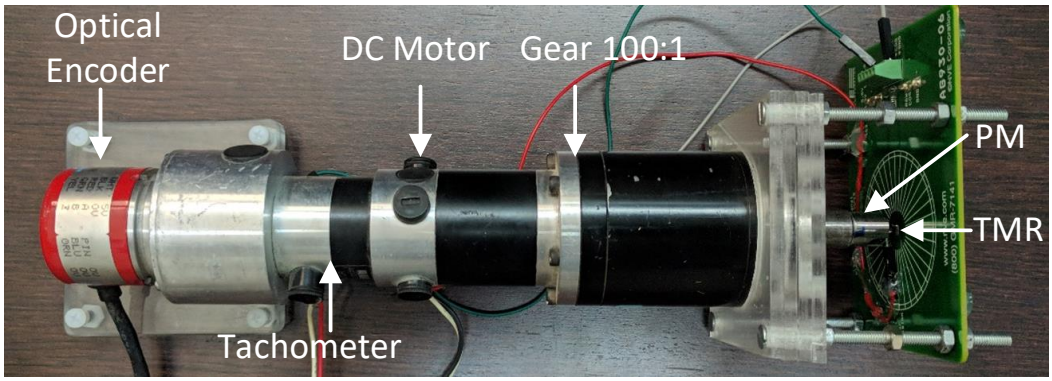

Figure 4.2. DC motor practical setup

The output of the Optical Encoder is fed directly into dSPACE PCC Special Encoder interface where its pulses will be counted and converted to a real angle. On the other hand, the sinusoidal outputs of the TMR sensor are conditioned through signal conditioning circuitry before being applied to the Analog-Digital-Converters ADCs of the dSPACE. The dSPACE then applies the selected converter and the imbalance correction technique and provide at its output signals proportional to the estimated angle ψ, the real angle θ, and $Error_\theta$ to test the converter's performance, Figure 4.3. In this chapter, the practical setup will be shown in detail along with the tests performed with it, results and their discussion.

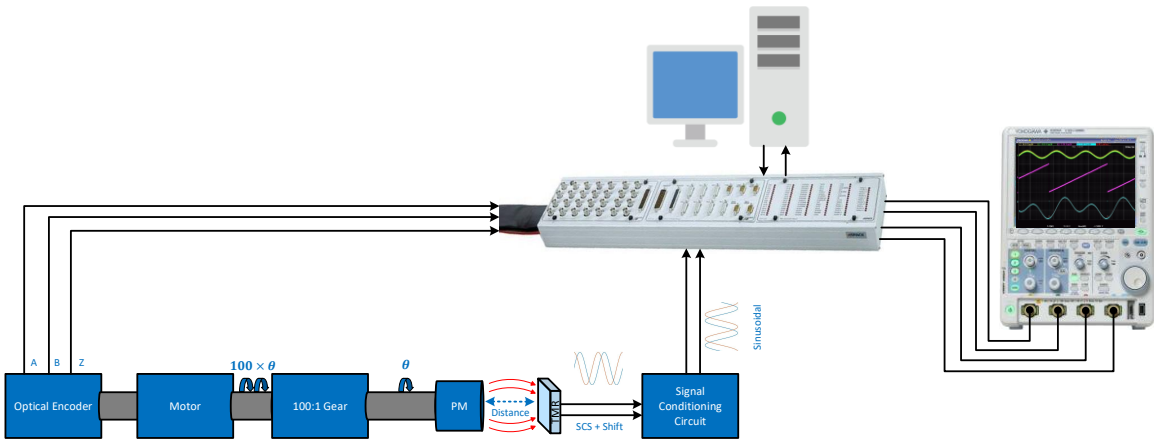

Figure 4.3. Practical setup block diagram

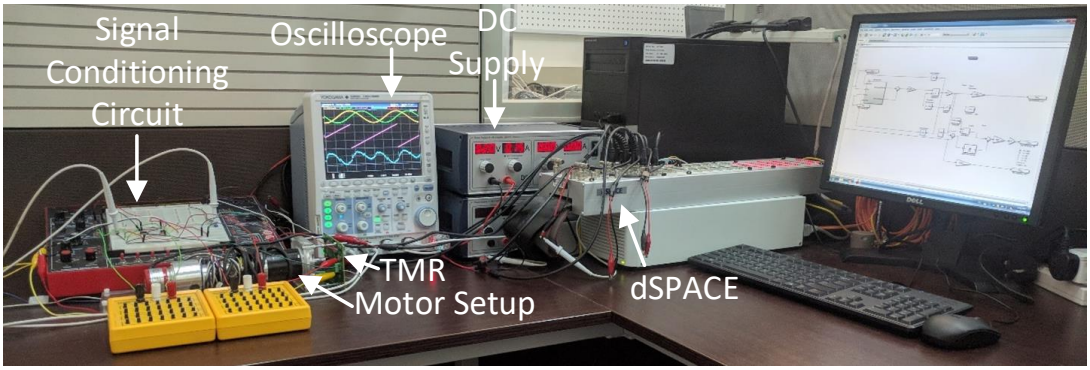

Figure 4.4. Practical setup

4.1.1 TMR Sensor

As discussed in chapter 2, the TMR sensor is resistive based [34], and thus it does not require a minimum supply voltage (V_{CC}) to operate. Yet, its maximum rating is 5.5V and preferred to work under 5V. The output signal will be shifted by half of the given V_{CC} in addition to 10mV per V_{CC}. Also, the Amplitude of the Sinusoidal output will be 100mv

per V_{CC} supplied. The Bridge resistance of the TMR sensor was reported to be in the range of Mega ohms under the effect of magnetic field, thus, the sinusoidal outputs will need to be buffered before any A/D conversion taking place. The effective magnetic field that can be applied to the sensor to ensure non-distorted results is reported to be $[30 - 200\ Oe]$. This claim will be tested in the upcoming section. [34] also mentioned that the sensor will usually have a $\pm 0.5°$ error if the sensor was at a fixed distance apart from the PM. Yet, it will lead to up to $\pm 3°$ of error if the distance between them is to vary. Since the sensor will be utilized at fixed distance from the PM, then it will be expected to have at least 0.5° error at the best case. The physical dimensions of the TMR sensor is $2.5 * 2.5 * 0.8\ mm$, which is very small compared to other angular position sensors as mentioned in chapter 1. The TMR sensor's Cosine and Sine branch's power supply come tied together, thus, necessary PCB alterations were done to accommodate for the proposed method as seen in Figure 4.5. Also, the package comes ready with an OP-AMP chip (TSV622) soldered on the PCB and used to buffer the two outputs of the sensor, as seen in the kit's circuit diagram; Figure 4.6. The chip was disconnected to allow for direct access to the raw Sin and Cosine signals of the TMR sensor and for appropriate usage of Instrumentation Amplifiers in later stage as seen in Figure 4.5.

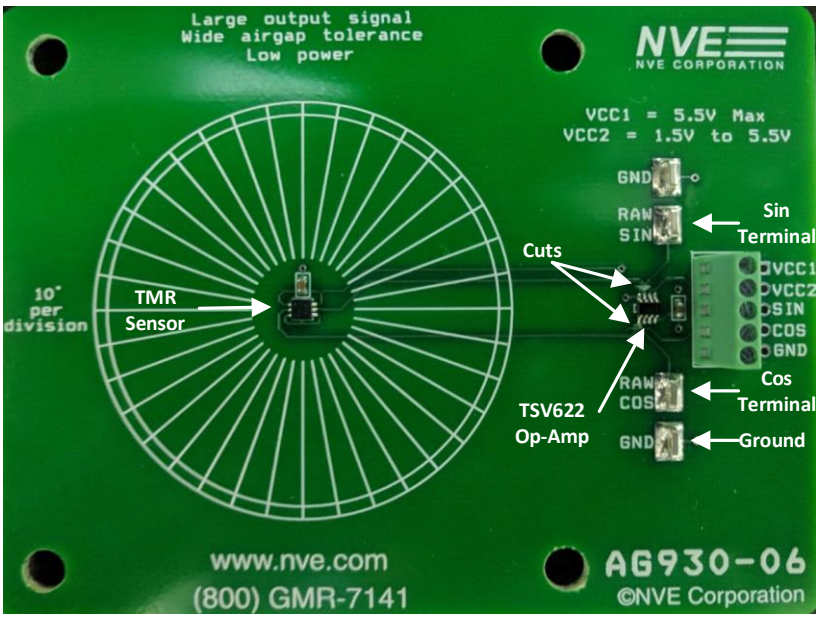

Figure 4.5. TMR PCB

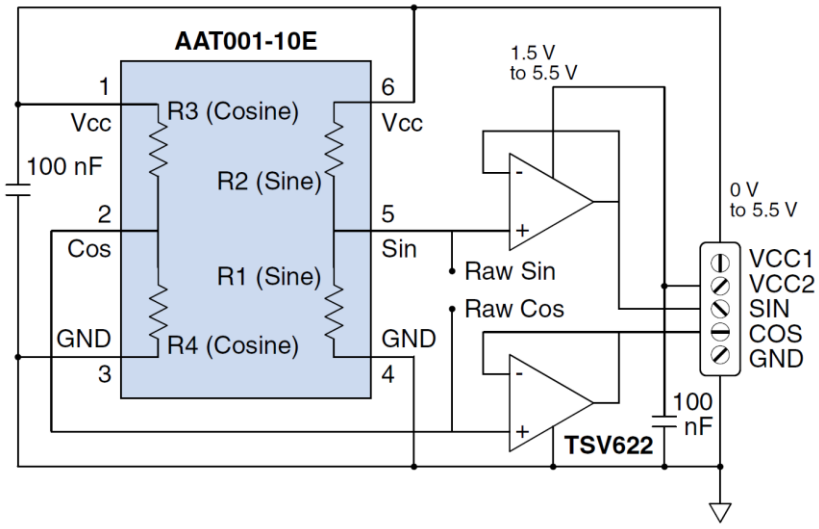

Figure 4.6. TMR kit circuit diagram, Source: [34]

4.1.2 Motor

The motor setup; from "Harmonic Drive" of the RH Mini Series, shown in Figure 4.2, incorporates a DC motor that is rated to run at 3000RPM and a maximum of 5000 RPM and a rated Output of 140 W. The gear used is 1:100 gear, and thus, the maximum rotational speed at the stepped down side is 50 RPM. On the other side, an Incremental Encoder is attached to the shaft, where it produces two quadrature outputs (A and B) that produce 1000 pulse per revolution, and thus 100k pulse per revolution at the stepped down side, which gives a resolution of $\frac{360^\circ}{100K} = 3.6^\circ \times 10^{-3}$. Also, the Optical Encoder comes ready with an absolute Zero reference terminal (Z) which outputs a pulse every revolution. The encoder is Open Collector type and should be powered through DC 5V power supply. The setup also comes ready with a Taco-meter, yet it will not be used for the upcoming tests.

4.1.3 Circuit

The conditioning circuit; shown in Figure 4.7, consists of two instrumentation amplifiers (IAs) "AD620" with an input impedance of $10G\Omega$, a gain of $G = 1 + \frac{49.4K\Omega}{R_G}$ and a minimum common mode rejection ratio (CMRR) of $-100dB$; at $G = 10$.

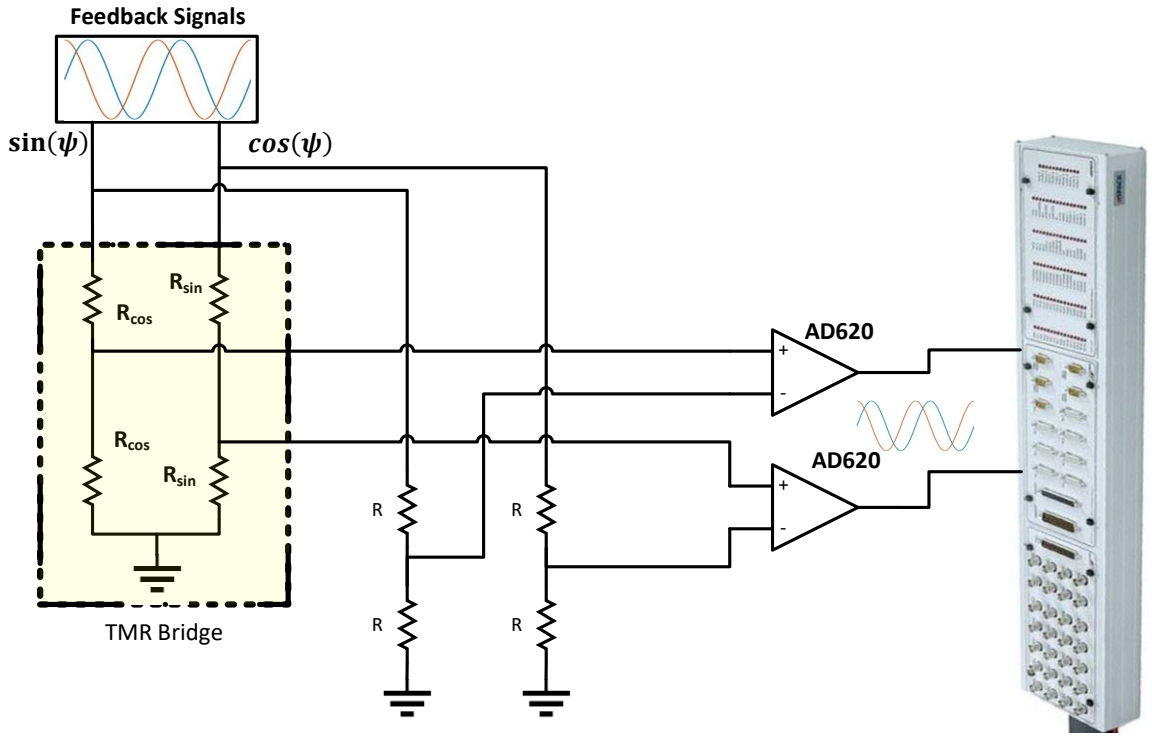

Figure 4.7. Signal conditioning circuit diagram

The instrumentation amplifiers remove the bias; i.e. $\left(\frac{\sin(\psi)}{2} + V_{Offset}\right)$ and $\left(\frac{\cos(\psi)}{2} + V_{Offset}\right)$, from the sensor signals and amplify the net Theta-related components; i.e. $\sin(\theta)\cos(\psi)$ and $\cos(\theta)\sin(\psi)$. The amplification gain was chosen to boost the sensors' signals to best match the dSPACE ADC range, yet, a safety margin was kept since the output signals of the sensor will heavily depend on the feedback of the loop, which in turn may overshoot at high speeds or at the beginning when motion is started. The amplitude of the sinusoidal outputs of the sensor are $100mV/V$ relative to their supply voltage,V_{CC}. As the maximum V_{CC} allowed is $5.5V$, thus, the maximum amplitude of the

sensor output anticipated should be $550mV$. Therefore, Gain G and R_G were chosen to be $G = 13$ and $R_G = 2k\Omega$ respectively. Accordingly, the outputs of the signal conditioning circuitry should have an amplitude of $A = 13 * 550mV = 7.15V$. The IAs provide a great buffering stage to the sinusoidal outputs along with other benefits such a Gain to match the ADC range of the dSPACE to reduce the quantization error. The Voltage division circuits were implemented through potentiometers in order to fine tune the voltage division to completely deduct the additive signals. Through the excellent CMRR of the IA, the subtraction should eliminate most of the additive signal at the output along with the $50Hz$ noise produced by the power lines and surrounding electrical equipment.

4.1.4 dSPACE

The platform used to test the proposed methods was dSPACE; shown in Figure 4.3. Namely, DS1003 board was used. It consists of multiple FPGAs, processors, ADC/DAC interfaces as well as multiple GPIOs and other analog/digital interfaces. It is used through PowerPC type: PPC 750GX, and has a CPU clock of 1GHZ. It has 16 ADC, where each 4 are time multiplexed through 4 Sample and hold circuits. Thus, 4 ADCs can be run simultaneously, which is needed for our application. Each ADC has a resolution of 16 bits, which is a great plus and has a range of $\pm 10\ V$, which gives a resolution of $res = \frac{10}{2^{16-1}} = 0.3mV$. The ADC conversion time is $1\mu s$ as reported, which should not be a problem for the application. The ADC also has $\pm 5mV$ offset error and 0.25% gain error. The DAC unit consists of 8 independent channels, each of 16 bits of resolution and $\pm 10V$ of range, which gives the same resolution of the ADC if utilized fully. The conversion time for ADC is $5\mu s$ and it has $\pm 1mV$ of offset error as well as 0.5% of gain error. The Digital Incremental

Encoder Interface however incorporates 6 independent decoders; only one will be utilized, the interface has 24bits of resolution and runs on $1.65MHz$ frequency. The interface includes pins that reads the quadrature outputs of the Incremental Encoder (A and B) as will as the Zero index output (Z). The interface is also capable of powering 5V/1.5A-Open Collector type encoders, which suits the Encoder used. The PLL method was implemented on the board with a minimum solver fixed step size of $7.5\mu s$.

4.2 Harmonic / Distance Test

Many tests were undergone on the TMR before proceeding with using it. These tests were essential to record its behavior for different sources of errors. Although Harmonic imbalance is usually neglected in the literature, as the sensors; regardless of their orientation, should feel only one rotational frequency, the PM's rotational frequency. The harmonic interference is highly tied with the distance between the PM and TMR sensor. Although TMR's sinusoidal behavior is theoretically independent of such distance but the direction only; yet, in practice, the distance would affect the magnetic flux intensity felt by the sensor and in turn, its output's frequency behavior. Thus, the optimal distance will be explored through searching for the distance that yields the minimum Harmonic Distortion of the outputs while testing within a set range of distances. The optimal distance will ensure a minimal harmonic interference but cannot completely null it.

Three distances will be shown for the distance test, namely, the results of the optimal distance in addition to other results of nearer and further distances to show the difference among different distances. The sensor's Sinusoidal output waveforms will be

shown along with their respective Lissajous (XY) and spectrum plots. Lissajous (XY) plots of harmonic free quadrature sinusoidal signals should be a perfect circle. Any addition of harmonic distortion will morph the circle into other shapes, depending on the amplitude and frequency of the distorting signal; and thus, it will be a good indicator of harmonic distortion. For this test, the motor was rotating at almost 40 rev/sec. Hence, the fundamental frequency is expected to be around $f_0 = \frac{1}{40} = 25mHz$. Subsequently, the third harmonic should be around $f_3 = 75mHz$. Figure 4.8 shows the result of the optimal distance found. It can be seen that the waveforms are sinusoidal in shape, Lissajous plot is very near to circular shape and the spectrum is showing a peak around $30mHz$ with $13.2dBV$ while the third harmonic was around $80mHz$ and with an amplitude of $-38.8dBV$. Thus, the third harmonic is around 0.25% of the fundamental signal. It is important to point that the oscilloscope's frequency resolution is $10mHz$, and thus, it was not able to capture $25mHz$ and $75mHz$, and captured $30mHz$ and $80mHz$ respectively instead.

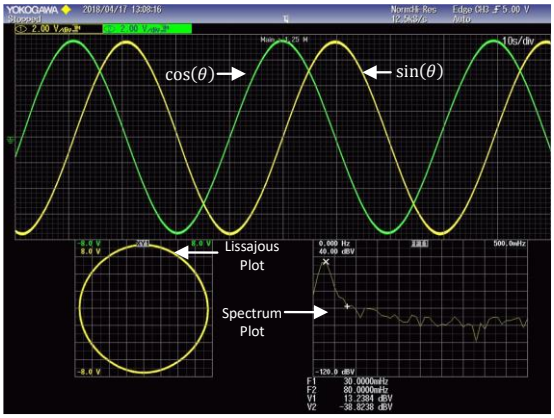

Figure 4.8. Optimal distance's sinusoidal waveform, Lissajous and spectrum

Figure 4.9 (left) shows a result of a short distanced TMR sensor. It can be seen that the waveform has morphed into a triangular shape waveform, and the Lissajou is not a circle anymore, instead, it developed four corners. Looking at the spectrum, it can be seen that the third harmonic is more dominant than that of the optimal result with an amplitude of $-13.6\,dBV$; which is around 4.8% of the fundamental frequency. Figure 4.9 (right) however, shows the result of a further displaced TMR sensor. It can be clearly seen that the waveform is very distorted and the Lissajou plot was morphed into a square shape as oppose to a perfect circle. The spectrum even reveals the harmonic nature of the waveforms as more harmonics emerged; i.e. 5^{th}, 7^{th}, etc. The third harmonic is calculated to be 9.5% of the fundamental frequency.

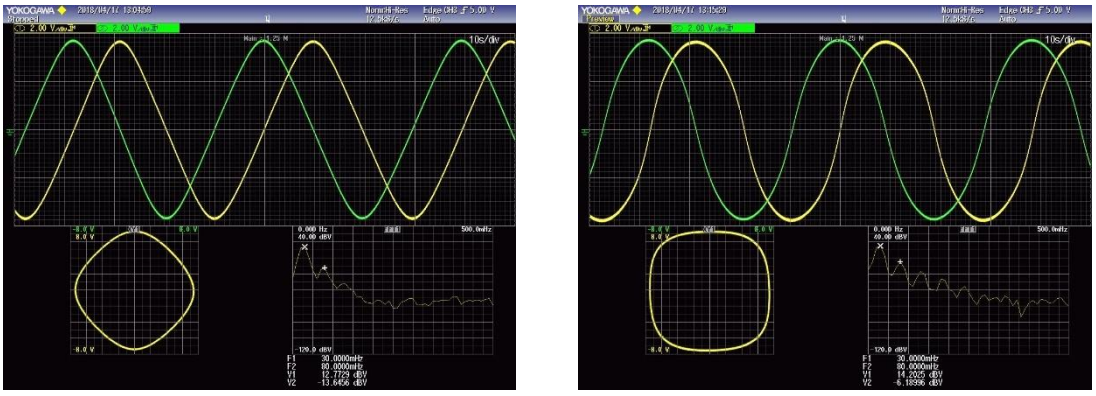

Figure 4.9. Near distanced (left) and far distanced (right) sinusoidal waveform, Lissajous and spectrum

In conclusion, it is shown that the distance between the TMR and the PM is very vital and should be carefully set to get the minimum harmonic distortion possible. The minimum distortion was found to be 0.25% third harmonic.

4.3 Practical results

4.3.1 Sensor Emulation

Sensor Emulation is very important to test the proposed method in a semi-controlled environment of errors and imbalances. It may also give an indication; along with previously done simulations; on how should the converter work under several conditions and how would the $Error_\theta$ waveform look like in such cases. In order to perform sensor emulation, a platform should produce two quadrature sinusoidal signals along with the angular position encoded within them and multiply them with the power supply provided; the feedback signals in our case, then output the modulated signals for the converter to decode them. Ideally, the platform used for emulation should be separated from the platform of the converter, yet, it was difficult to afford another dSPACE board to emulate the sensor separately from the PLL converter. Thus, the emulation process was done within the same dSPACE board, then the modulated signals were outputted through the board's DACs and inputted again through its ADCs for conversion to take place. Then the $Error_\theta$ was generated by subtracting the estimated angle ψ and the original signal θ. The emulation tests will test the $\alpha/DC/\phi$ imbalances simulated earlier as in Table 3.1. The emulation was done under the same aforementioned simulation conditions; i.e. $A = 7.5$ and ran under 1 rev/sec. First, a perfect imbalance free test was done, shown in Figure 4.10

(top) to test for the best-case error. The Yellow and Green waveforms are for the modulated $\sin(\theta)$ and $\cos(\theta)$ respectively. The purple waveform is the estimated angle ψ and the light blue signal is the $Error_\theta$ waveform. Please note that every result may vary in the order of magnitude of error, and thus, those who got very small $Error_\theta$ were scaled up from within the dSPACE to match the DAC range of operation, and vice versa for large $Error_\theta$. Figure 4.10 (top) shows an $Error_\theta$ waveform of 4.68° PP error that was upscaled 500 times, and thus the real error of perfect emulation is $4.68° \times 10^{-3}$. Figure 4.10 shows that the combined error is expected to have a PP $Error_\theta$ of $0.7° - 2.35°$ under the test conditions.

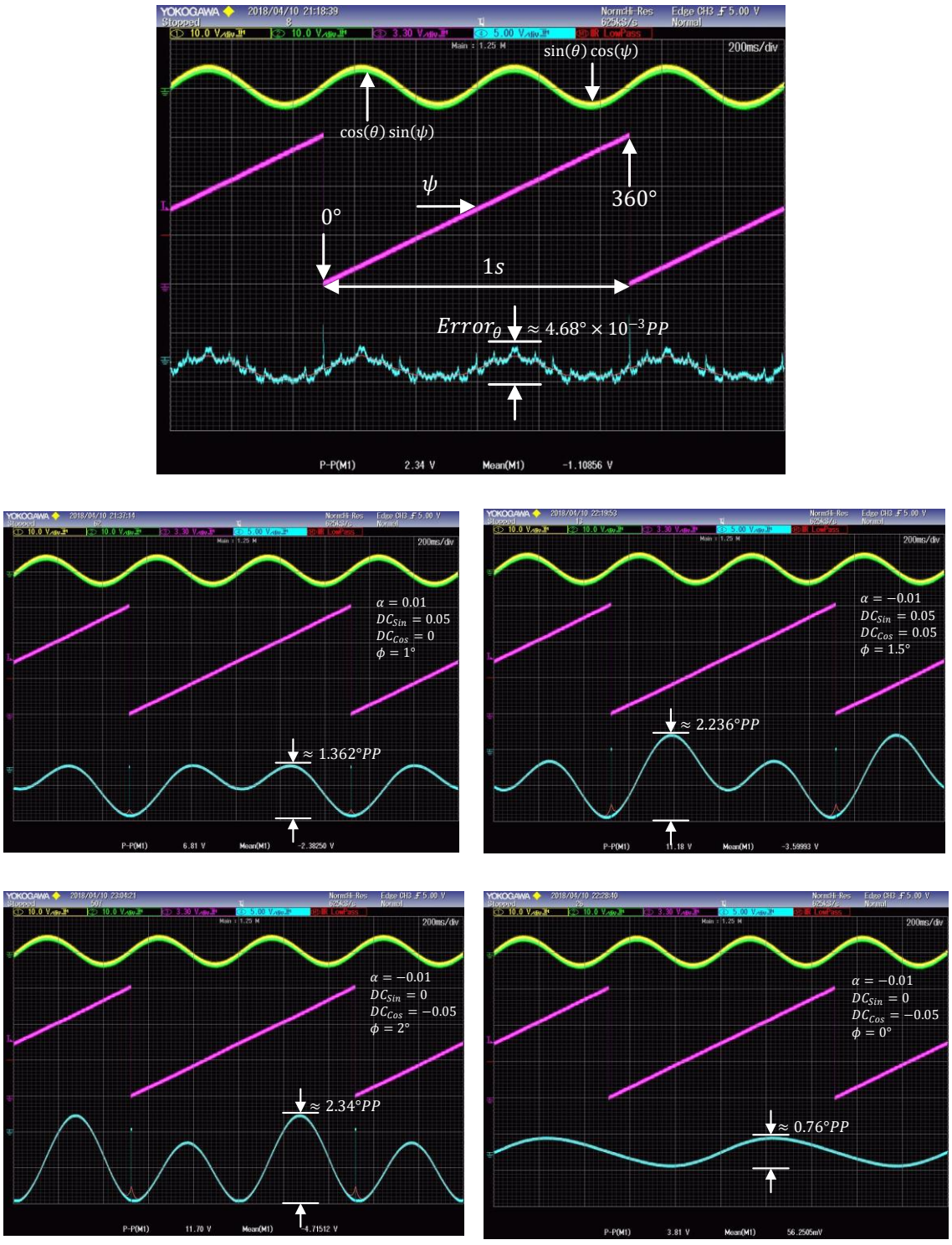

Figure 4.10. Emulation results of perfect imbalance free scenario (top) and scenarios (1.1-1.4) in order from left to right

4.3.2 Practical Results on TMR Sensor

As mentioned before, in order to assess the performance of the proposed method practically in terms of $Error_\theta$, the optical encoder quadrature signals were used; as its resolution was calculated to be $3.6° \times 10^{-3}$. The dSPACE Incremental Encoder interface was used to count the pulses. Then, the counted pulses were divided by the gear ratio; 100, and the pulses per revolution; 1000, and then multiplied by 360 to acquire the real angle. Then, in order to eliminate the initial phase shift between the encoder and the TMR sensor. A condition was made to synchronize. It tracks the output angle of the converter ψ until it reaches zero, at that moment, it forces the counter to reset to 0 counts. This process happens every 3 revolutions to insure synchronization. This method does not utilize the Zero index pin of the Optical Encoder (Z) as it gets triggered 100 times per 1 revolution of the main shaft. After having both signals synchronized, the $Error_\theta$ waveform; light blue on oscilloscope figures, will be generated by subtracting them from each other. Side note, the main shaft was chosen to run at low speeds as the dSPACE program was not able to keep up with the high input rate of the optical encoder's pulses. Thus, all tests were run at around 40s/revolution.

Since all of the methods mentioned in the literature review for TMR sensor was Open Loop based, it was unfair to compare the proposed method's performance to them. Thus, it was decided to compare it to the classical PLL's performance. At the best case scenario, the proposed method should should yield the same $Error_\theta$ performance as that of the classical PLL.

Towards that, the TMR sensor was supplied by fixed 4V DC signal and its

sinusoidal output signals were then supplied to the Classical PLL Converter implemented on the dSPACE. Figure 4.11 (a) and (b) show the performance of the Classical PLL. It is shown that the PP $Error_\theta$ is 1.99° when the imbalances were not compensated and 1.255° when compensated for. It is worth pointing out that the Figure 4.11 $Error_\theta$ waveform shows only two peaks, which initially gave the illusion that the signals were free of harmonic interference, yet, when correction took place, two extra peaks emerged, which suggests that a harmonic interference were present since the beginning, yet, it was overshadowed by other imbalances' errors as shown in Scenario 2.6 in the previous chapter. As mentioned earlier in the distance / harmonic test, the 3rd harmonic distortion is almost 0.25% of the fundamental, which explains the $Error_\theta$ waveform PP error based on the simulations done. It is worth mentioning that the phase correction technique used was the proposed phase correction method, not the classical method.

On the other hand, the proposed method showed a PP $Error_\theta$ of 1.98° and 1.245° before correction and after correction respectively. Which is almost identical to the $Error_\theta$ performance shown for classical PLL. Likely, the $Error_\theta$ waveform had only two peaks before any imbalance correction taking place while having 4 peaks after correction. Which reinforces the fact that the error was due to the Harmonic interference, and that it in line with the ± 0.5 error reported for fixed gap setup within the TMR's datasheet.

Therefore, the results suggest that the proposed method is practically working and would yield to nearly 0 PP $Error_\theta$ if the Harmonic imbalances were not present and other imbalances were corrected for. It also suggests that the proposed phase imbalance method is also practically working for both classical and proposed enhanced PLL techniques.

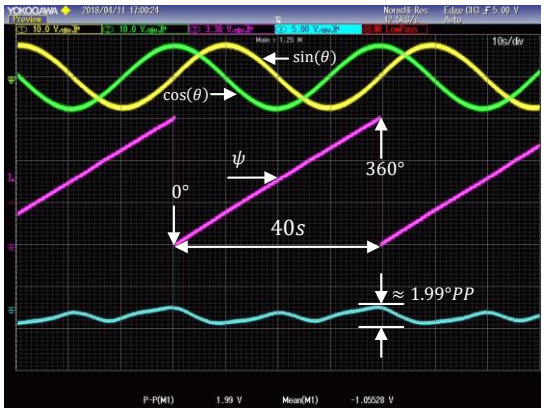

(a)

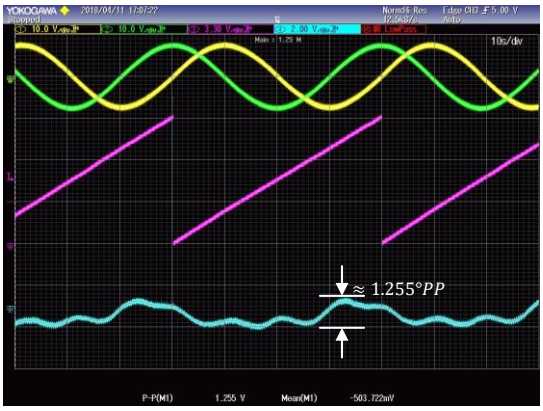

(b)

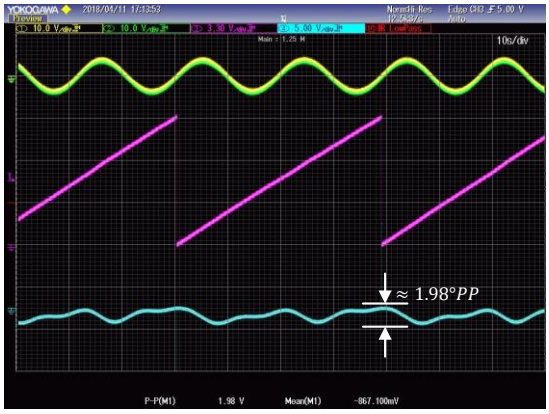

(c)

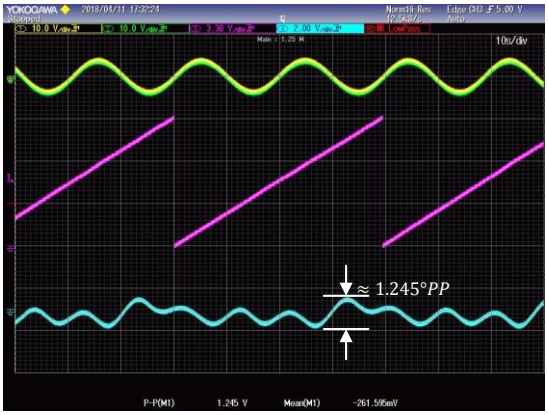

(d)

Figure 4.11. Classical PLL (top) VS Proposed enhanced PLL (bottom) Practical Results Unbalanced Classical PLL (a), Balanced Classical PLL (b), Unbalanced Proposed PLL (c) and Balanced Proposed PLL(d).

CHAPTER 5: CONCLUSION

5.1 Conclusions

In conclusion, a sinusoidal angular position sensor, namely magneto resistive sensor, was chosen according to its merits against other encoders. Such sensors come with two drawbacks, first, their non-linear relationship with respect to the angle of rotation θ. Second, imperfections such as imbalances, which, if left uncorrected will induce high error in the instrumentation. In order to learn about the state of the art advances in MR sensors conversion techniques, a literature review was undergone. It was found that all of works found in literature were open loop converters. As open loop converters are vulnerable to instability issues and not usually robust, it was thought to contribute to such field by proposing a novel closed loop converter along with a suitable signal imbalance correction technique. The proposed closed loop technique was an enhanced PLL. The enhancement done was towards lowering the complixity of the classical PLL by eliminating one of its most expensive elements, analog multipliers. The proposed method exploits the MR sensor's power supply to feedback the VCO signals through them. Thus, the output sinusoidal signals will be inherently multiplied by the feedback signals, instead of the need of analog multipliers to carry out the multiplication operation. Consequently, new imbalance correction techniques were proposed to fit the proposed converter, as conventional correction methods will not be suitable. The proposed techniques were then extensively tested under controlled, semi-controlled and with real TMR sensor situations. The proposed methods were proven to be fully functioning and having a performance similar to that of the classical methods. Practically, both proposed PLL and classical

methods resulted in around 1.2° PP error which was then proven to be the result of an inevitable 3rd harmonic distortion within the sensor.

5.2 Future Work

As it was shown that harmonic interference and other sorts of imbalances may result in a significant error, it is proposed to dedicate more work towards precisely detecting such errors and compensating for them fully. Also, more attention should be given to harmonic interference, as it is a real issue with MR sensors in general as opposed to other sinusoidal encoder sensors.

REFERENCES

[1] M. Gasulla, X. Li, G. C. M. Meijer, L. Van der Ham, and J. W. Spronck, “A contactless capacitive angular-position sensor,” *IEEE Sens. J.*, vol. 3, no. 5, pp. 607–614, 2003.

[2] Y. Zhang, D. Zheng, W. Xing, and S. Fan, “Design of IIR filter in capacitive rotary position sensor based on FPGA,” *2012 8th IEEE Int. Symp. Instrum. Control Technol. ISICT 2012 - Proc.*, no. 1, pp. 143–146, 2012.

[3] D. Zheng, S. Zhang, S. Wang, C. Hu, and X. Zhao, “A capacitive rotary encoder based on quadrature modulation and demodulation,” *IEEE Trans. Instrum. Meas.*, vol. 64, no. 1, pp. 143–153, 2015.

[4] N. A. Qamar, C. J. Hatziadoniu, and H. Wang, “Speed error mitigation for a DSP-based resolver-to-digital converter using autotuning filters,” *IEEE Trans. Ind. Electron.*, vol. 62, no. 2, pp. 1134–1139, 2015.

[5] M. Benammar and A. S. P. Gonzales, “A novel PLL resolver angle position indicator,” *IEEE Trans. Instrum. Meas.*, vol. 65, no. 1, pp. 123–131, 2016.

[6] M. Caruso, A. O. Di Tommaso, F. Genduso, R. Miceli, and G. R. Galluzzo, “A DSP-Based Resolver-To-Digital Converter for High-Performance Electrical Drive Applications,” *IEEE Trans. Ind. Electron.*, vol. 63, no. 7, pp. 4042–4051, 2016.

[7] S. Leroy, S. Rigert, A. Laville, A. Ajbl, and G. F. Close, “Integrated Hall-Based Magnetic Platform for Position Sensing,” pp. 360–363, 2017.

[8] D. Rapos, C. Mechefske, and M. Timusk, “Dynamic sensor calibration: A comparative study of a Hall effect sensor and an incremental encoder for measuring shaft rotational position,” *2016 IEEE Int. Conf. Progn. Heal. Manag. ICPHM 2016*, 2016.

[9] Y. Y. Lee, R. H. Wu, and S. T. Xu, “Applications of linear Hall-effect sensors on angular measurement,” *Proc. IEEE Int. Conf. Control Appl.*, pp. 479–482, 2011.

[10] S. Das, T. S. Sarkar, B. Chakraborty, and H. S. Dutta, “A simple approach to design a binary coded absolute shaft encoder,” *IEEE Sens. J.*, vol. 16, no. 8, pp. 2300–2305, 2016.

[11] Q. H. Wan, Y. Y. Wang, Y. Sun, and S. W. Yang, “A novel miniature absolute metal rotary encoder based on Single-track Periodic Gray Code,” *Proc. 2012 2nd Int. Conf. Instrum. Meas. Comput. Commun. Control. IMCCC 2012*, pp. 399–402, 2012.

[12] Y. Chen, M. Yang, J. Long, D. Xu, and F. Blaabjerg, “M/T Method based Incremental Encoder Velocity Measurement Error Analysis and Self-Adaptive Error Elimination Algorithm,” in *IECON 2017 - 43rd Annual Conference of the IEEE Industrial Electronics Society*, 2017, pp. 2085–2090.

[13] N. K. Bhaskarrao, C. S. Anoop, and P. K. Dutta, “A Simple Signal Conditioner for Tunneling Magneto-Resistance based Angle Sensor,” pp. 1–6, 2016.

[14] N. K. Bhaskarrao, C. S. Anoop, and P. K. Dutta, “A Linearizing Interface Circuit with Phase-Error Compensated Direct-Digital Output for TMR- Based Angular Position Sensor,” 2017.

[15] N. K. Bhaskarrao, C. S. Anoop, and P. K. Dutta, “A simple and efficient front-end circuit for Magneto-resistive angle sensors,” *I2MTC 2017 - 2017 IEEE Int. Instrum. Meas. Technol. Conf. Proc.*, 2017.

[16] A. Zambrano and H. G. Kerkhoff, “Online digital compensation Method for AMR sensors,” in *2016 IFIP/IEEE International Conference on Very Large Scale Integration, VLSI-SoC 2016*, 2016, no. 2, pp. 1–4.

[17] A. Zambrano and H. G. Kerkhoff, “Online digital offset voltage compensation method for AMR sensors,” in *2015 IEEE International Instrumentation and Measurement Technology Conference (I2MTC)*, 2015, pp. 1512–1515.

[18] A. Khattab, M. Benammar, and F. Bensaali, “A Novel method for online correction of amplitude and phase imbalances in sinusoidal encoders signals,” in *2016 IEEE*

International Power Electronics and Motion Control Conference (PEMC), 2016, pp. 784–789.

[19] W. Thomson, “On the Electro-Dynamic Qualities of Metals:--Effects of Magnetization on the Electric Conductivity of Nickel and of Iron,” *Proc. R. Soc. London*, vol. 8, no. 0, pp. 546–550, 1856.

[20] M. N. Baibich *et al.*, “Giant Magnetoresistance of (001)Fe/(001)Cr Magnetic Superlattices,” *Phys. Rev. Lett.*, vol. 61, no. 21, 1988.

[21] G. Binasch, P. Grünberg, F. Saurenbach, and W. Zinn, “Enhanced magnetoresistance in layered magnetic structures with antiferromagnetic interlayer exchange,” *Phys. Rev. B*, vol. 39, no. 7, pp. 4828–4830, 1989.

[22] M. Julliere, “Tunneling between ferromagnetic films,” *Phys. Lett. A*, vol. 54, no. 3, pp. 225–226, 1975.

[23] T. Miyazaki and N. Tezuka, “Giant magnetic tunneling effect in Fe/Al2O3/Fe junction,” *J. Magn. Magn. Mater.*, vol. 139, no. 3, pp. 94–97, 1995.

[24] J. S. Moodera, L. R. Kinder, T. M. Wong, and R. Meservey, “Large magnetoresistance at room temperature in ferromagnetic thin film tunnel junctions,” *Phys. Rev. Lett.*, vol. 74, no. 16, pp. 3273–3276, 1995.

[25] S. Andreev and P. Dimitrova, “Anisotropic- magnetoresistance integrated sensors,” *J. Optoelectron. Adv. Mater.*, vol. 7, no. 1, pp. 199–206, 2005.

[26] M. Parkin, S, Jiang, X., Kaiser, C., Panchula, A., Roche, K., Samant, “Magnetically Engineered Spintronics Sesnors and,” *Proc. IEEE*, vol. 91, no. 5, pp. 661–680, 2003.

[27] Y. Tian and S. Yan, “Giant magnetoresistance: History, development and beyond,” *Sci. China Physics, Mech. Astron.*, vol. 56, no. 1, pp. 2–14, 2013.

[28] J. E. Lenz, “A review of magnetic sensors - Proceedings of the IEEE,” *Proc. IEEE*, vol. 78, no. 9036163, pp. 973–989, 1990.

[29] J. Lenz and A. S. Edelstein, “Magnetic Sensors and Their Applications,” *IEEE Sensors Journal2*, vol. 6, no. 3, pp. 631–649, 2006.

[30] A. E. Mahdi, L. Panina, and D. Mapps, “Some new horizons in magnetic sensing: High-TcSQUIDs, GMR and GMI materials,” *Sensors Actuators, A Phys.*, vol. 105, no. 3, pp. 271–285, 2003.

[31] J. C. S. Kools, “Exchange-biased spin-valves for magnetic storage,” *IEEE Trans. Magn.*, vol. 32, no. 4 PART 2, pp. 3165–3184, 1996.

[32] W. H. Butler, X.-G. Zhang, T. C. Schulthess, and J. M. MacLaren, “Spin-dependent tunneling conductance of Fe|MgO|Fe sandwiches,” *Phys. Rev. B*, vol. 63, no. 5, p. 54416, 2001.

[33] J. Mathon and A. Umerski, “Theory of tunneling magnetoresistance of an epitaxial Fe/MgO/Fe(001) junction,” *Phys. Rev. B*, vol. 63, no. 22, p. 220403, 2001.

[34] “AAT001-10E TMR Angle Sensor,” *Components*. .

[35] C. S. Anoop, B. George, and K. V. Jagadeesh, “Tunneling magneto-resistor based angle transducer,” *Proc. Int. Conf. Sens. Technol. ICST*, pp. 431–435, 2011.

[36] B. George, V. J. Kumar, and A. Chandrika Sreekantan, “Analysis of a tunnelling magneto-resistance-based angle transducer,” *IET Circuits, Devices Syst.*, vol. 8, no. 4, pp. 301–310, 2014.

[37] C. S. Anoop, B. George, and V. Jagadeesh Kumar, “A linear Tunneling Magneto-Resistance angle transducer,” *2012 IEEE I2MTC - Int. Instrum. Meas. Technol. Conf. Proc.*, pp. 2073–2077, 2012.

[38] C. S. Anoop and B. George, “Electronic scheme for computing inverse-cosine and its application to a GMR based angle sensor,” *IEEE Trans. Instrum. Meas.*, vol. 61, no. 7, pp. 1991–1999, 2012.

[39] C. S. Anoop and B. George, “A novel signal conditioning scheme for magneto-resistive

angle sensors," *2012 IEEE I2MTC - Int. Instrum. Meas. Technol. Conf. Proc.*, pp. 2083–2087, 2012.

[40] C. S. Anoop, S. Member, and B. George, "New Signal Conditioning Circuit for MR Angle Transducers With Full-Circle Range," vol. 62, no. 5, pp. 1308–1317, 2013.

[41] M. Benammar and A. S. P. Gonzales, "Position Measurement Using Sinusoidal Encoders and All-Analog PLL Converter with Improved Dynamic Performance," *IEEE Trans. Ind. Electron.*, vol. 63, no. 4, pp. 2414–2423, 2016.

[42] N. Al-Emadi, L. Ben-Brahim, and M. Benammar, "A new tracking technique for mechanical angle measurement," *Meas. J. Int. Meas. Confed.*, vol. 54, pp. 58–64, 2014.

[43] C. Mohan, R. Sivappagari, and N. R. Konduru, "M ODIFIED ATO A LGORITHM BASED H IGH."

[44] C. Sivappagari, N. Konduru, and S. Theil, "High Tracking Accuracy of Software Based RDC Using Various Excitation Signals," *Sp. Technol.*, no. October, p. 2003, 2014.

[45] N. Noori and D. A. Khaburi, "A new software-based method for rotor angle calculation," *PEDSTC 2014 - 5th Annu. Int. Power Electron. Drive Syst. Technol. Conf.*, no. Pedstc, pp. 305–310, 2014.